# Static and dynamic modeling of a UPS system in an IP topology

**Auteur :** Hedia, Kevin
**Promoteur(s) :** Van Cutsem, Thierry
**Faculté :** Faculté des Sciences appliquées
**Diplôme :** Master en ingénieur civil électricien, à finalité approfondie
**Année académique :** 2015-2016
**URI/URL :** http://hdl.handle.net/2268.2/1441

UNIVERSITY OF LIÈGE - FACULTY OF APPLIED SCIENCES

MASTER THESIS

# Static and Dynamic Modeling of a UPS System in an IP Topology

Author:
Kevin Hedia

Master thesis advisors:
Pr Thierry Van Cutsem
Dr Patrick Scarpa

Graduation Studies conducted for obtaining the Master's degree in Electrical Engineering

Academic year 2015-2016

# Abstract

Title : Static and Dynamic Modeling of a UPS System in an IP Topology

Author: Kevin Hedia

Master thesis advisors: Pr Thierry Van Cutsem and Dr Patrick Scarpa

Master in Electrical Engineering

Academic year 2015-2016

This master thesis analyzes the behavior of Diesel Rotary Uninterruptible Power Supply (DRUPS) baptized NO-BREAK KS® built and configured by EURO-DIESEL. Once the technical specifications is acquired by the electrical engineering department, studies must be carried with respect to the number and power ratings of DRUPS and the network topology, within which the DRUPS will be installed, chosen by the customer.

The guidelines of this master thesis include two main objectives.

The first objective of the master thesis is to create a program in SCILAB to perform a power flow analysis in which the DRUPS are placed within an Isolated Parallel (IP) topology where the value of the IP choke is important for the isolation of the units. The program must also be able to compute several scenarios to evaluate the redundancy level of the system and the fault study. Through the program, we can see that increasing the value of the IP choke, the voltage drop grows exponentially at a load terminal (Figure 1). Therefore, we can notice that the value of the IP choke limits the transmitted power to this load.

The second objective is to examine the dynamic modeling, by using RAMSES software, of the NO-BREAK KS® to accurately analyze the transitional period. The numerical simulation of the dynamic response of the NO-BREAK KS® allows the analysis of the rotor speed which is fundamental to detect instability. The simulation of this instability will be done through sudden load variation. To illustrate these results, two cases will be considered: a load variation of 1 MW with a very high value of IP choke (Figure 2) and a load variation of 6 MW with a low value of IP choke (Figure 3).

In conclusion, the program allows electrical engineers to perform studies of electrical quantities, pre-fault and post-fault, in the IP topology. Moreover, the developed dynamic models in this master thesis represent rather well the behavior of the NO-BREAK KS® at the time of occurrence of one or more disturbances and to check whether the electrical system is still stable or not.
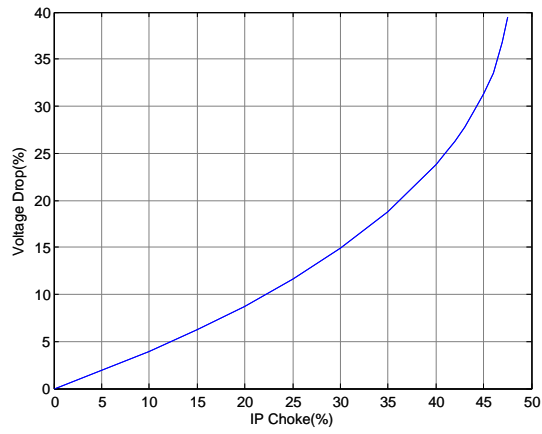
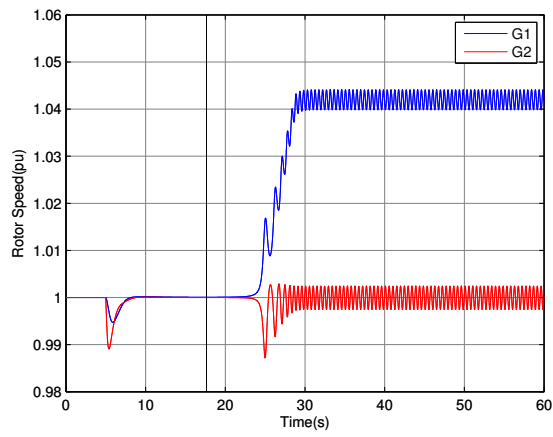Figure 1: Evolution of Voltage Drop with respect to the IP Choke



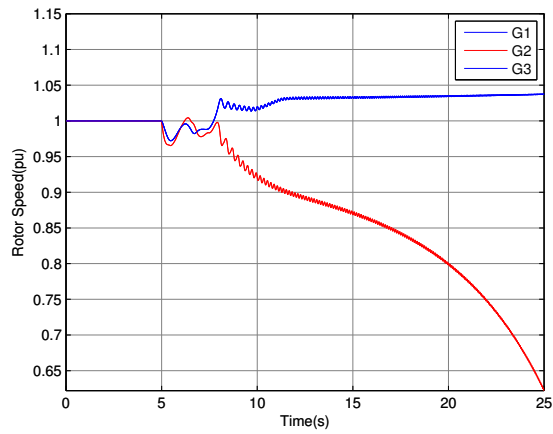Figure 2: Evolution of the Rotor Speed with respect to time



Figure 3: Evolution of the Rotor Speed with respect to load variation

# Acknowledgement

*I would like to take this opportunity to thank everyone who supported me throughout this master thesis, I am thankful for the time they have given me, for their advice, constructive criticism and technical support.*

*First of all I express my gratitude to my master thesis advisors Professor Thierry Van Cutsem and Doctor Patrick Scarpa, for their patience, guidance, and immense knowledge. They accompanied me in my efforts and supervised my progress throughout this work. I thank them for the confidence they always testified me.*

*I thank the team of EURO-DIESEL who have helped and supported me to carry this master thesis. And I would especially like to express my gratitude to Vincent Defosse, Quentin Dejace, Georges Romischer and Luc Thiteux.*

*Then I would like to thank the PhD students of Prof. Thierry Van Cutsem : Lampros Papangelis and Tilman Weckesser who were always available during the development of this work.*

*Before concluding, I would like to thank all the Professors of Faculty of Applied Sciences. And especially the Professors Patricia Rousseaux and Christophe Geuzaine who agreed to be part of my jury.*

*And last but not least, I thank my friends and family.*

# Contents

# List of Figures

# List of Tables

# Introduction

## Statement of the Problem and Objective of the Master Thesis

EURO-DIESEL is a private company established in 1989 from the province of Liège, Belgium, by a team of innovators who specialized in critical power systems [1]. EURO-DIESEL ensures power supply security for major businesses and industries worldwide by building and configuring a Diesel Rotary Uninterruptible Power Supply (DRUPS) system baptized the NO-BREAK KS®. But EURO-DIESEL also sells to their customers, along with their DRUPS, control panels and power panels.

Once the technical specifications is acquired by the electrical engineering department, studies must be carried with respect to the number and power ratings of DRUPS and the network topology, within which the DRUPS will be installed, chosen by the customer. More precisely, a part of these studies evaluates the redundancy level of the system by means of several scenarios and another part consists in studying the impact of a fault on the electrical quantities. On completion of these studies, the engineer can conclude whether the case is feasible or not.

In this context, the guidelines of my master thesis include two main objectives.

The first objective of the master thesis is to create a program in SCILAB (an open source, cross-platform numerical computational package and a high-level, numerically oriented programming language [2]) to perform a power flow analysis in which the DRUPS are placed within an Isolated Parallel (IP) topology. The program must also be able to compute several scenarios to evaluate the redundancy level of the system and the fault study. The main features of the program should be fast, efficient and ergonomic.

The second objective is to examine the dynamic modeling of the NO-BREAK KS® to accurately analyze the transitional period. The numerical simulation of the dynamic response of the NO-BREAK KS® has, so far, never been investigated by EURO-DIESEL.

## Structure of the Work

In the first chapter, we introduce the basics of how the NO-BREAK KS® works whose purpose is to supply immediately the critical loads in case of an outage.

The second chapter explains the different topologies used by EURO-DIESEL and more precisely, the IP topology whose main objective is to secure critical loads for high power ratings at low voltage and to reduce the short-circuit current.

In chapter three, we introduce the theoretical background of the power systems analysis methods. These latter will be recall in three steps. The first step recalls the theoretical basis of the Newton-Raphson procedure for the power flow study. The second step recalls the theoretical background of sensitivity analysis which numerically allows to directly know how the output voltage of the UPS system influences the load voltage. The last step recalls the theoretical background of the fault study which is divided into two main parts : the analysis of balanced faults and the analysis of unbalanced faults.

In chapter four, we will show the results of different numerical models that I developed using SCILAB based on the power systems analysis methods. This chapter will be divided into three parts. The first part will show the program implementation and the flowchart of the program. While the second part deals with the validation of my numerical models. Finally, we will apply my program for the full study of a practical problem provided by EURO-DIESEL.

The fifth chapter will introduce the RAMSES software as well as how to use CODEGEN utility via a structured file needed for the creation and addition of a new model in RAMSES.

The sixth chapter will describe the models developed for the excitation and torque controls to simulate the behavior of the NO-BREAK KS®.

In chapter seven, the models will be used in RAMSES to simulate the response of the NO-BREAK KS®. The first section of this chapter will compare the response of the numerical models to the real response of the NO-BREAK KS® while the second section will explore the stability limits of the system.

The main conclusions about the contribution of this work is summarized in chapter eight. Following annexes which include the specific data to which the reader may refer. And finally, the main references in order of appearance in this thesis.

# Part I

# Euro-Diesel's UPS and IP Topology

# Chapter 1

# Introduction To The NO-BREAK KS® System [3]

EURO-DIESEL manufacture a Diesel Rotary Uninterruptible Power Supply (DRUPS) system called the NO-BREAK KS® whose purpose is to secure immediately the supply of critical loads in case of an outage.

The package sold by EURO-DIESEL is shown in Figure 1.1, as can be seen there are two main parts : the control and power panels and the DRUPS. In this section, only the DRUPS operation will be explained despite the fact that the control and power panels are crucial components but it is not necessary for the understanding of the continuation of this master thesis.
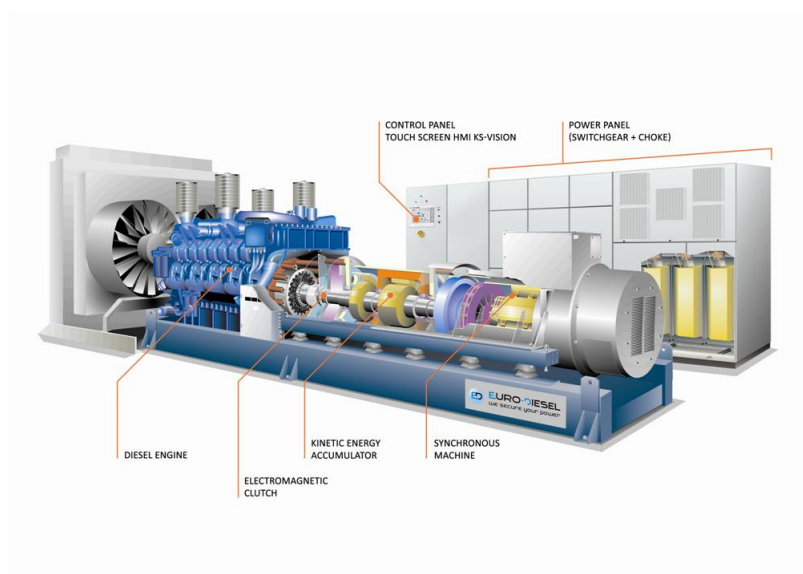


Figure 1.1: Package Sold by EURO-DIESEL

As one can observe, the DRUPS is composed of four main parts : the diesel engine, the electromagnetic clutch, the kinetic energy accumulator and the synchronous machine. However, The diesel engine is not the main expertise of EURO-DIESEL, indeed, the main expertise is the assembly of the kinetic energy accumulator and the synchronous machine. These latter are displayed with more details in Figure 1.2. In fact, the combination is called Stato-Alternator.
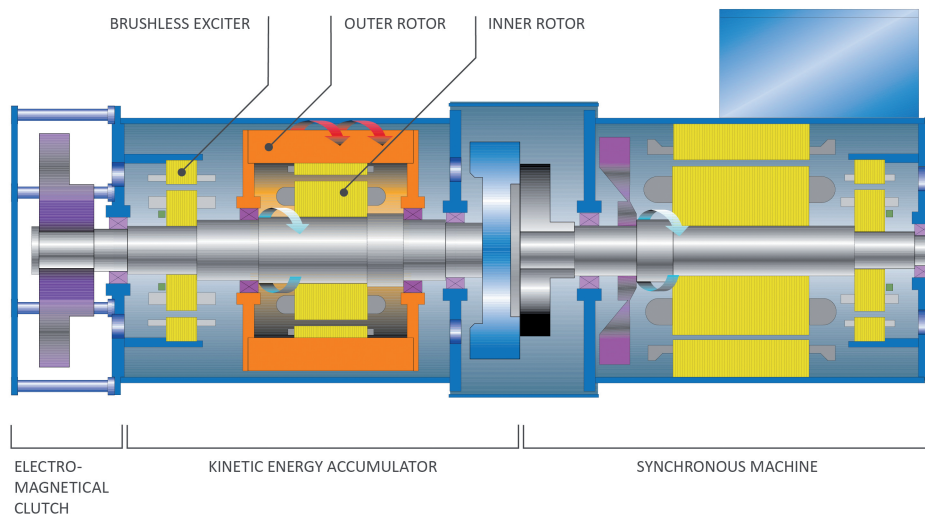


Figure 1.2: The Stato-Alternator

For the synchronous machine sub-part, the rotor is a salient 4-pole rotor and the exciter is a brushless and ringless technology that uses an AC alternator and rotating rectifiers to produce the DC field required.

For the kinetic energy accumulator sub-part, it is composed of two rotating parts : an inner rotor and an outer rotor. The inner rotor is rotating at 1500 rpm or 1800 rpm and contains two sets of windings : a three-phase AC winding and a DC winding. It is also a brushless and ringless exciter which supplies these windings. Concerning the outer rotor, it runs mechanically-free around the inner rotor which stores kinetic energy. During the first moment of a power outage, the kinetic energy stored in the outer rotor supplies the load until the diesel engine reached the rated speed.

The DRUPS can be operate in three different states : conditioning mode, transient period and independent mode.

In conditioning mode, the synchronous machine is supplied by the mains and acts as a motor which drives the main shaft and thus the inner rotor. The AC winding of the inner rotor is supplied in order to generate a rotating magnetic field that induced eddy currents at the windings of the outer rotor and thus, the latter can reach the maximum speed of 3000 rpm. However, since the inner rotor is already rotating at 1500 rpm, the AC winding needs to feed with a current of a frequency of 50Hz. So the outer rotor stores kinetic energy.

In the transient period, directly after a power outage, the DC winding of the inner rotor is supplied which, in consequence, will create a magnetic coupling between the inner and outer rotor. Since the outer rotor has stored some kinetic energy, it will be transferred through this coupling in a controlled manner to keep the inner rotor at nominal speed. This transient period secure the critical loads until the diesel engine is ready to take over.

In independent mode, the diesel engine is at the rated speed and is ready to take over. There is then a coupling between the stato-alternator and the diesel engine via an electromagnetic clutch. The diesel engine provides the power to the load for an indeterminate time. During this mode, The outer rotor is accelerated to 3000 rpm again and stores the kinetic energy to its full capacity.

# Chapter 2

# IP System Philosophy [4-5]

The IP topology stands for "Isolated Parallel topology". The main objective is to secure critical loads for high power ratings (above 5MVA) at low voltage, instead of medium voltage. For application where load power ratings is exceeding 2.75 MVA, a parallel topology is recommended. As a matter of fact, the most powerful DRUPS build by EURO-DIESEL is a 2.75 MVA DRUPS in 50 Hz.

## 1    Parallel Topology

In Figure 2.1, a low voltage parallel topology is shown with a common load and 3 units. As discussed above, this configuration can supply bigger power demands as well as the required (N + 1) and/or (N + 2) redundancy levels.
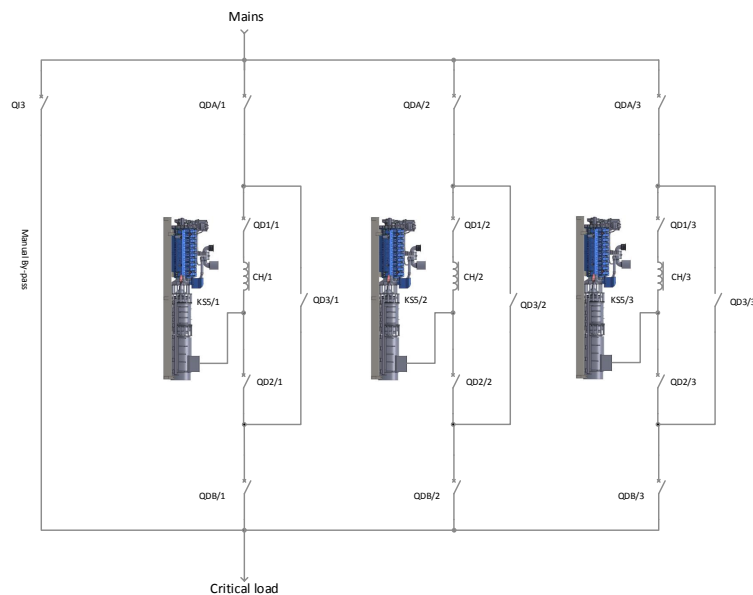


Figure 2.1: Parallel Topology - Low Voltage

Due to its simple and reliable design, this configuration is used for many applications such as supplying large datacenters facilities. However, when the power consumed by the load increases, exceeding 5 MVA, more DRUPS systems need to be paralleled, which can lead to high short-circuit currents. Therefore, one needs to adapt the switchgears due to the high value of short-circuit current, hence these latter become very specific and expensive. A mean to overcome this effect is to pass from low voltage to medium voltage.

In Figure 2.2, a medium voltage configuration is shown. The advantage of that configuration is that it holds the same intrinsic high reliability than the low voltage parallel configuration.
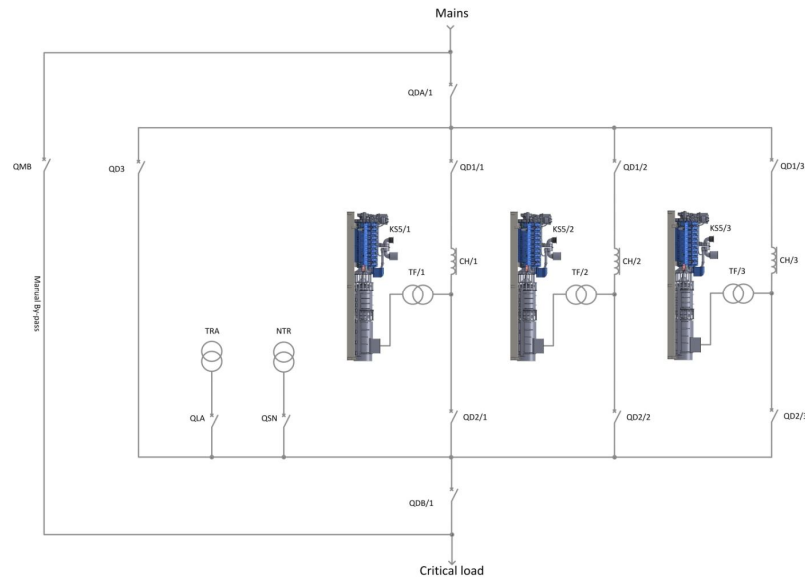


Figure 2.2: Parallel Topology - Medium Voltage

However, one can keep a low voltage configuration by adding circuit breakers and chokes called IP chokes. Two network topologies has been developed : IP Star topology and IP Ring topology.

## 2    IP Topology

The IP topology is subdivided into two parts : the IP star and the IP ring. These topologies are implemented in the program that I developed during my master thesis.

### 2.1    IP Star

The IP Star configuration is shown in Figure 2.3, this latter differs from the parallel configuration shown in Figure 2.1. In this topology, each DRUPS has a downstream load, it is no longer a common load shared by the DRUPS as the parallel topology. All loads are connected, through a choke called IP Choke, to a bus

named the IP Bus.

However, this configuration requires additional breakers and, thus, the complexity increases to ensure the suitable functioning of the network .

The two modes of operation will be detailed hereafter : The conditioning mode and the independent mode.
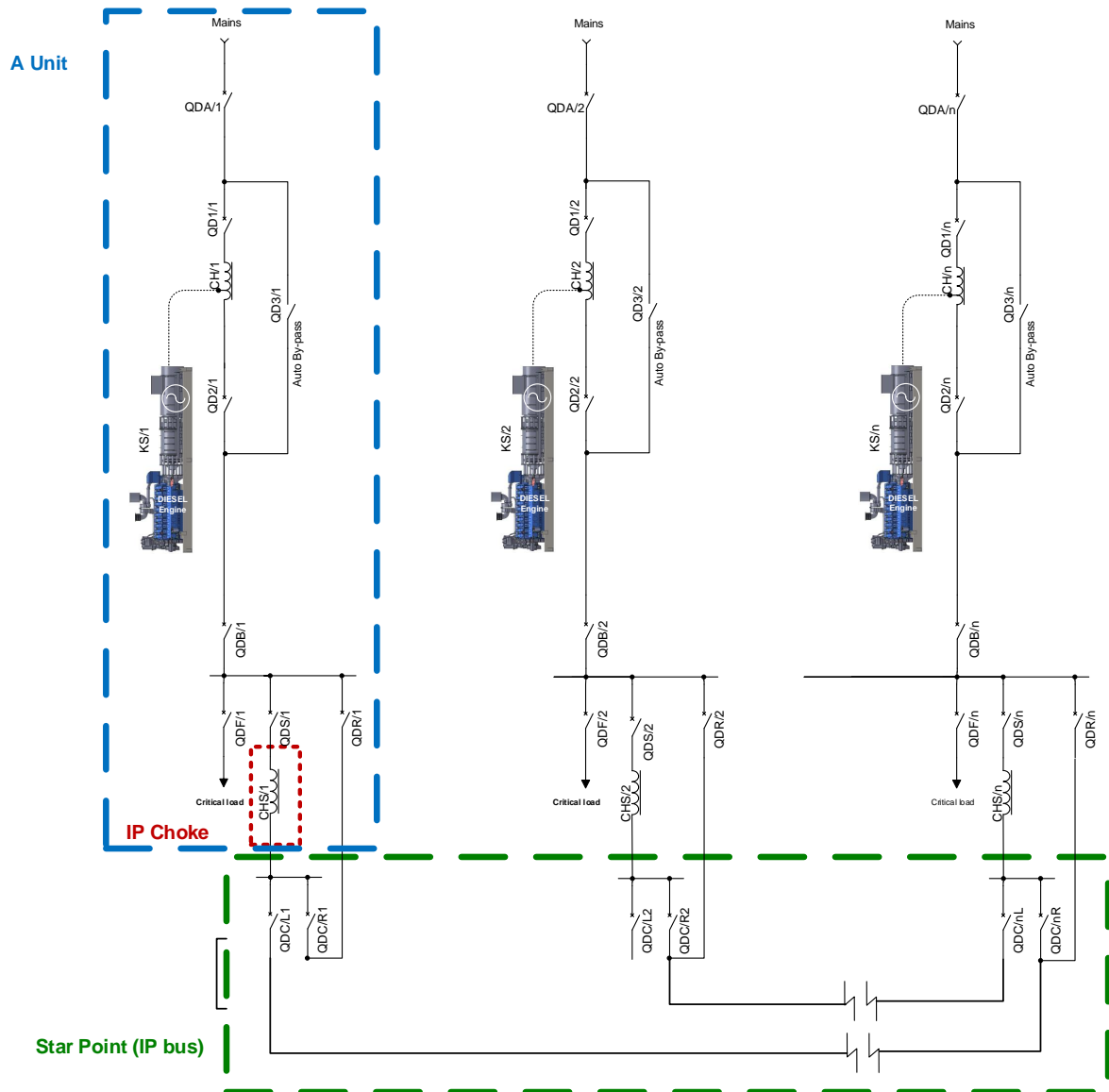


Figure 2.3: IP Star Topology

**Conditioning Mode**

The conditioning mode corresponds to the "normal" operating mode, that is to say, when the mains is still present. Starting from Figure 2.3, several breakers are closed such as : QDA/x, QD1/x, QD2/x, QDB/x, QD-S/x, QDF/x, QDC/xL and QDC/xR. Others are left open such as QD3/x and QDR/x. The resulting topology is shown in Figure 2.4.
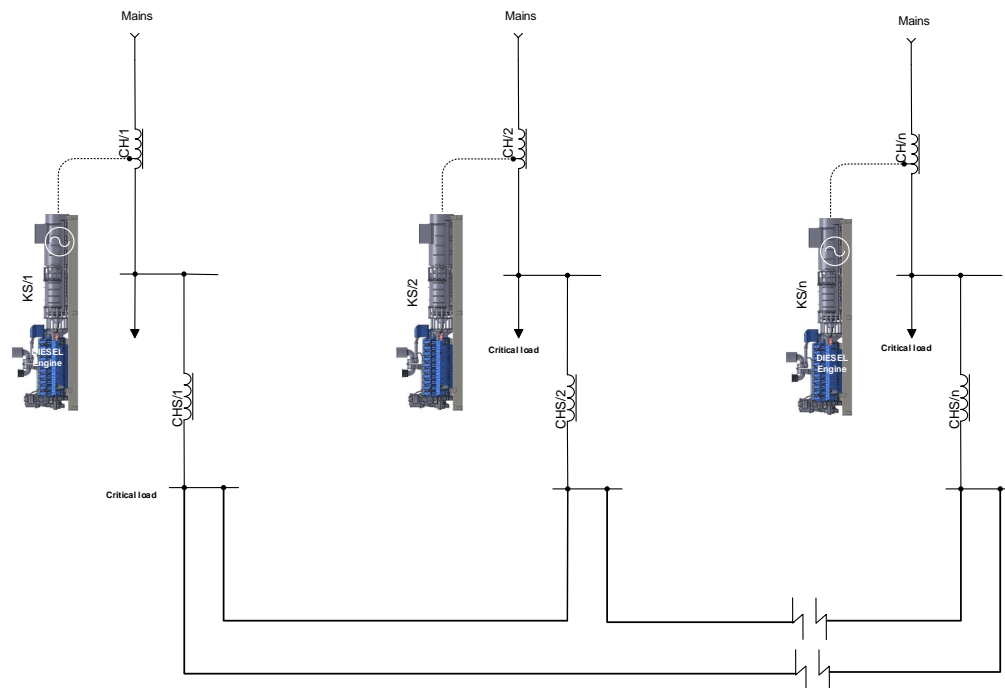


Figure 2.4: IP Star Topology - Conditioning Mode

The DRUPS are used as synchronous condensers, their utility is to keep the load voltage at 1 per unit (pu) by tuning their excitation system. In fact, the load's active power is supplied by the mains and the DRUPS consumed a few kilowatts. In the one hand, if the loads is evenly spread between the units, there is no currents flowing through the IP chokes. On the other hand, if the loads are not balanced, active power sharing occurs between the units and currents flow in the ring. As regards the reactive power, it is limited by the IP chokes which is of the order of 30% in the per unit system.

**Independent Mode**

In Figure 2.5, one can see the independent mode. Once a mains failure is detected, the breakers QD1/x open and the DRUPS become synchronous generators. The active power is distributed equally between machines, they work in unison. However, reactive power sharing is disabled, each DRUPS is regulating their downstream load voltage independently of the others.
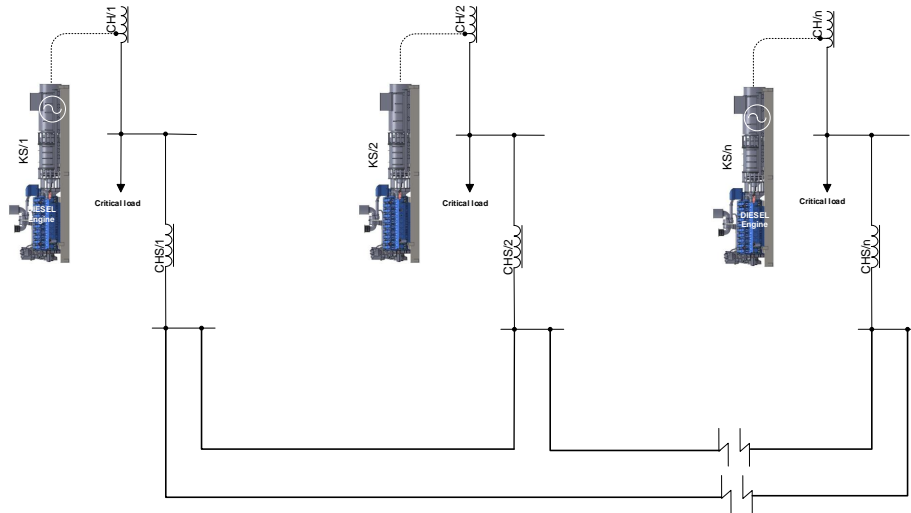
Figure 2.5: IP Star Topology - Independent Mode

The two events that follow the setting off of a unit i are : the opening of QD2/i and then the closing of QDR/i. The IP star configuration is usually designed as a redundant system and the downstream load of the unit which is put out of service is supplied through the IP choke during the first moments. The voltage of that load will rapidly drop and, thus, the IP choke impedance should be kept as low as possible. When the QDR/x is closed, the IP choke is short-circuited and the load is placed on the IP bus as can be seen in Figure 2.6.
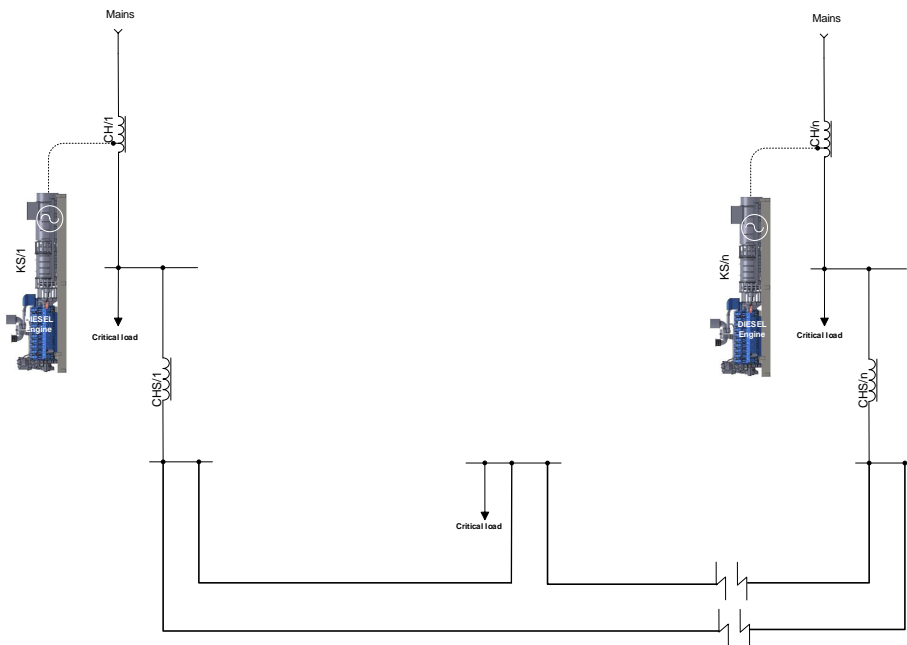


Figure 2.6: IP Star Topology - Conditioning Mode when a KS tripped

## 2.2 IP Ring

The Isolated Parallel ring (IP ring) topology, shown in Figure 2.7, is slightly different than the IP star topology. Indeed, the IP Choke is no longer between the load and the IP bus but between two successive loads on the IP bus. However, the philosophy remains the same, this topology has been designed to allow protection of low voltage loads while limiting the short-circuit currents involved and still providing redundancy. This particular topology is applicable for at most four units.
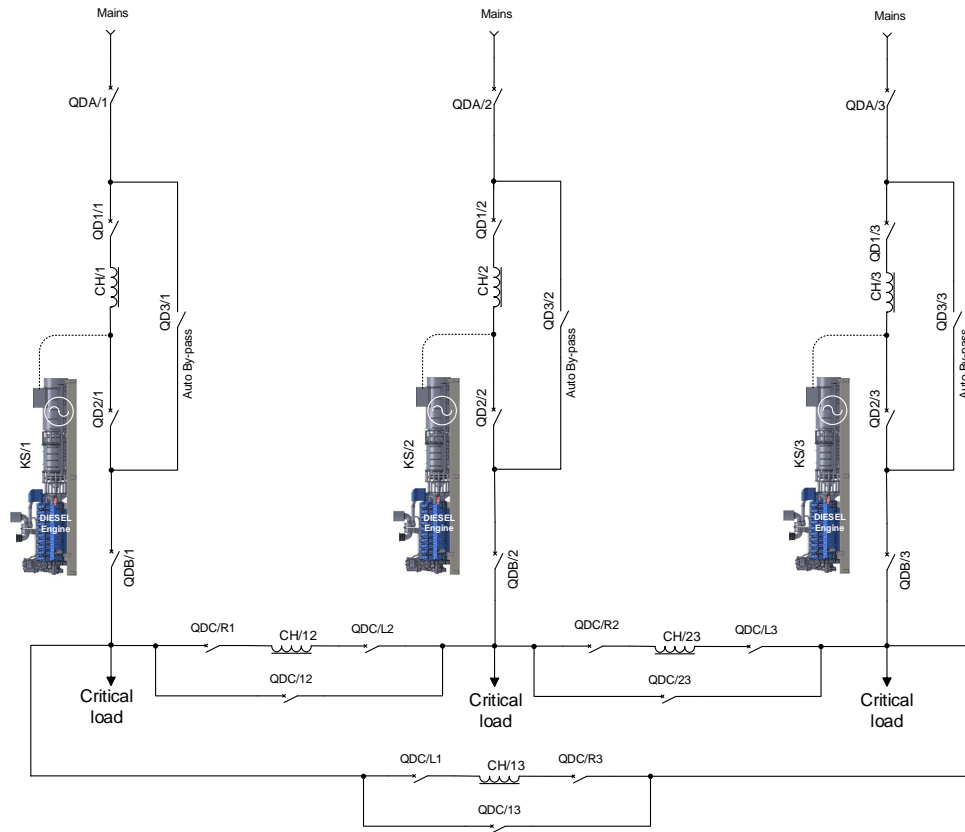
Figure 2.7: IP Ring Topology

# Part II

# Static Modeling

# Purpose of This Part

The main objective of the part that we will study is to compute the steady state electrical quantities in two different topologies.

To succeed, this part will include two chapters. The first will focus to implement the theoretical background of the power systems analysis. Then the second chapter will show the results of different numerical models that I developed using SCILAB. We will check that the results provided by my program correspond with good accuracy to the results provided a power flow software and then apply my program to a practical case study.

# Chapter 3

# Recall of the Power Systems Analysis Methods

## 1   Power flow [6]

The main goal of EURO-DIESEL is to secure the supply of electrical energy for their customer load. Pre-analysis must be perform in order to know the voltage magnitudes and phase angles for a set of buses in the IP topology.

A way to solve the problem is to apply a specific procedure to the power flow problem. Since the power flow equations are non-linear, one needs an iterative procedure to solve the problem. In this context, the Newton-Raphson method is chosen due its computational robustness.

Thereafter, the theoretical basis of the Newton-Raphson procedure will be detailed and then applied to the power flow formulation to solve the EURO-DIESEL's problem.

### 1.1   The Newton-Raphson Procedure

In fact, the Newton-Raphson method finds the roots of non-linear algebraic system of equations. It requires successive approximations to reach the real solution. It is called iterative root finding procedure.

The procedure starts by an initial guess. In this particular problem, due to the small number of buses in the network, a flat start can be chosen. The latter is when the voltage magnitudes of buses are set to 1 pu and the phase angles are set to 0. This first guess is usually incorrect, an updated of the guesses is needed in order to converge towards the solution.

Several methods exist to solve the power flow problem such as Gauss-Seidel method but Newton-Raphson method has become, most of the time, the de-facto industry standard [6]. The main reason is that the convergence properties of this method are pretty good even if it begins with a flat start. Moreover, it converges quadratically.

Let reminds the mathematically basis of the Newton-Raphson method.

**Newton Raphson for the Multidimensional Case**

Assume we have n nonlinear algebraic equations and n unknowns. A first initial guess $\underline{x}^{(0)}$ is made but since it is a guess, $\underline{f}(\underline{x}^{(0)}) \neq 0$. An update of the solution is required. Let denotes $\Delta\underline{x}^{(0)}$ the variation of the solution which will make $\underline{f}(\underline{x}^{(0)} + \Delta\underline{x}^{(0)}) = 0$.

The NR procedure is based on the Taylor series expansion of the functions $\underline{f}(\underline{x})$ :

$$\underline{f}(\underline{x}^{(0)} + \Delta\underline{x}^{(0)}) = \underline{f}(\underline{x}^{(0)}) + \underline{f}'(\underline{x}^{(0)})\Delta\underline{x}^{(0)} + \frac{1}{2}\underline{f}''(\underline{x}^{(0)})(\Delta\underline{x}^{(0)})^2 + ... = 0 \qquad (3.1)$$

Higher order terms are small and can be neglected assuming that guess is a good enough such that $\Delta\underline{x}^{(0)}$ is small. So,

$$\underline{f}(\underline{x}^{(0)} + \Delta\underline{x}^{(0)}) = \underline{f}(\underline{x}^{(0)}) + \underline{f}'(\underline{x}^{(0)})\Delta\underline{x}^{(0)} = 0 \qquad (3.2)$$

At this point, the Jacobian matrix can be introduced. The latter stores all the derivatives for each individual function with respect to each individual unknown. So for the $k^{th}$ function and the $j^{th}$ unknown, the term of the Jacobian is $\frac{\partial f_k(\underline{X}^{(0)})}{\partial x_j}$.

Since we have n functions and n unknowns, the Jacobian matrix should be of size nxn :

$$
J = \begin{bmatrix}
\frac{\partial f_1(\mathbf{X}^{(0)})}{\partial x_1} & \frac{\partial f_1(\mathbf{X}^{(0)})}{\partial x_2} & \cdots & \frac{\partial f_1(\mathbf{X}^{(0)})}{\partial x_n} \\
\frac{\partial f_2(\mathbf{X}^{(0)})}{\partial x_1} & \frac{\partial f_2(\mathbf{X}^{(0)})}{\partial x_2} & \cdots & \frac{\partial f_2(\mathbf{X}^{(0)})}{\partial x_n} \\
\vdots & \vdots & & \vdots \\
\frac{\partial f_n(\mathbf{X}^{(0)})}{\partial x_1} & \frac{\partial f_n(\mathbf{X}^{(0)})}{\partial x_2} & \cdots & \frac{\partial f_n(\mathbf{X}^{(0)})}{\partial x_n}
\end{bmatrix}
$$

From eq. (3.2) we have

$$
\underline{\mathbf{f}}'(\underline{\mathbf{x}}^{(0)})\Delta\underline{\mathbf{x}}^{(0)} = -\underline{\mathbf{f}}(\underline{\mathbf{x}}^{(0)}) \tag{3.3}
$$

From the equation above the term $\underline{\mathbf{f}}'(\underline{\mathbf{x}}^{(0)})$ is in fact the Jacobian, it becomes

$$
J\Delta\underline{\mathbf{x}}^{(0)} = -\underline{\mathbf{f}}(\underline{\mathbf{x}}^{(0)}) \tag{3.4}
$$

We can easily find $\Delta\underline{\mathbf{x}}^{(0)}$

$$
\Delta\underline{\mathbf{x}}^{(0)} = -J^{-1}\underline{\mathbf{f}}(\underline{\mathbf{x}}^{(0)}) \tag{3.5}
$$

Considering the small number of buses of the system, we can easily obtain the inverse of the Jacobian. However, in programming, a LDU decomposition is used to solve the problem for large system.

Since we know the variation of the state vector, we can update it

$$
\underline{\mathbf{x}}^{(1)} = \underline{\mathbf{x}}^{(0)} + \Delta\underline{\mathbf{x}}^{(0)} \tag{3.6}
$$

And finally, for any iteration

$$
\underline{\mathbf{x}}^{(i+1)} = \underline{\mathbf{x}}^{(i)} + \Delta\underline{\mathbf{x}}^{(i)} \tag{3.7}
$$

The basis of the Newton-Raphson procedure have been developed. Let now introduce the form of the admittance matrix for this application.

## 1.2 Admittance Matrix

We introduce the admittance matrix that relates current injections and the voltages at a bus. The Figure 3.1 shows a one-line diagram representation of the network that we study. More precisely, it represents the IP Star topology with one NO-BREAK KS® . This topology is normally used with two NO-BREAK KS® or more. For the sake of simplicity, we will derive the admittance matrix of this simple network and due to the symmetry of this topology, this admittance matrix will serve as sub-block for bigger admittance matrices.
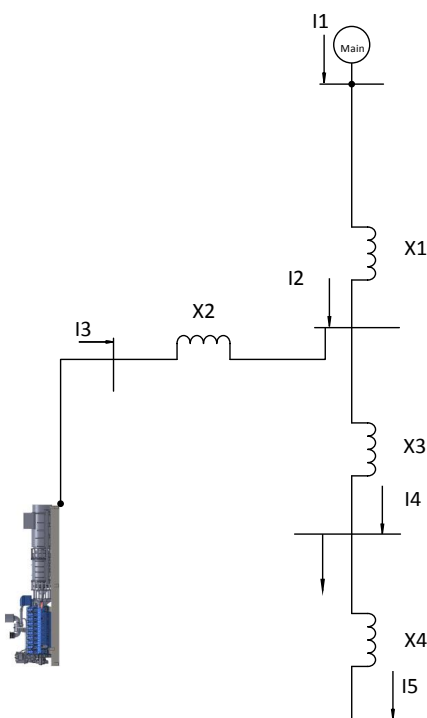


Figure 3.1: A Unit of the IP Star Topology

By Kirchoffs Current Law, one has

$$
\begin{cases}
\bar{I}_1 = (\bar{V}_1 - \bar{V}_2)\dfrac{1}{jX_1} \\[2mm]
\bar{I}_2 = (\bar{V}_2 - \bar{V}_1)\dfrac{1}{jX_1} + (\bar{V}_2 - \bar{V}_3)\dfrac{1}{jX_2} + (\bar{V}_2 - \bar{V}_4)\dfrac{1}{jX_3} \\[2mm]
\bar{I}_3 = (\bar{V}_3 - \bar{V}_2)\dfrac{1}{jX_2} \\[2mm]
\bar{I}_4 = (\bar{V}_4 - \bar{V}_2)\dfrac{1}{jX_3} + (\bar{V}_4 - \bar{V}_5)\dfrac{1}{jX_4} \\[2mm]
\bar{I}_5 = (\bar{V}_5 - \bar{V}_4)\dfrac{1}{jX_4}
\end{cases}
\tag{3.8}
$$

18

In order to simplify the writing, let use the admittance since $\frac{1}{X} = y$. The equations system becomes :

$$
\begin{cases}
\bar{I}_1 = y_{12}\bar{V}_1 - y_{12}\bar{V}_2 \\
\bar{I}_2 = (y_{21} + y_{23} + y_{24})\bar{V}_2 - y_{21}\bar{V}_1 - y_{23}\bar{V}_3 - y_{24}\bar{V}_4 \\
\bar{I}_3 = y_{32}\bar{V}_3 - y_{32}\bar{V}_2 \\
\bar{I}_4 = (y_{42} + y_{45})\bar{V}_4 - y_{42}\bar{V}_2 - y_{45}\bar{V}_5 \\
\bar{I}_5 = y_{54}\bar{V}_5 - y_{54}\bar{V}_4
\end{cases}
\tag{3.9}
$$

We may write the system of equations in matrix form :

$$
\begin{bmatrix} \bar{I}_1 \\ \bar{I}_2 \\ \bar{I}_3 \\ \bar{I}_4 \\ \bar{I}_5 \end{bmatrix} =
\begin{bmatrix}
y_{12} & -y_{21} & 0 & 0 & 0 \\
-y_{12} & y_{21} + y_{23} + y_{24} & -y_{23} & -y_{24} & 0 \\
0 & -y_{32} & y_{32} & 0 & 0 \\
0 & -y_{42} & 0 & y_{42} + y_{45} & -y_{45} \\
0 & 0 & 0 & -y_{54} & y_{54}
\end{bmatrix}
\begin{bmatrix} \bar{V}_1 \\ \bar{V}_2 \\ \bar{V}_3 \\ \bar{V}_4 \\ \bar{V}_5 \end{bmatrix}
$$

So we have the admittance matrix

$$
\mathbf{Y} =
\begin{bmatrix}
y_{12} & -y_{21} & 0 & 0 & 0 \\
-y_{12} & y_{21} + y_{23} + y_{24} & -y_{23} & -y_{24} & 0 \\
0 & -y_{32} & y_{32} & 0 & 0 \\
0 & -y_{42} & 0 & y_{42} + y_{45} & -y_{45} \\
0 & 0 & 0 & -y_{54} & y_{54}
\end{bmatrix}
$$

Denoting the element in row i, column j, as $Y_{ij}$, the latter becomes element of the admittance matrix rather than an admittance.

$$
Y =
\begin{bmatrix}
Y_{11} & Y_{21} & 0 & 0 & 0 \\
Y_{12} & Y_{22} & Y_{23} & Y_{24} & 0 \\
0 & Y_{32} & Y_{33} & 0 & 0 \\
0 & Y_{42} & 0 & Y_{44} & Y_{45} \\
0 & 0 & 0 & Y_{54} & Y_{55}
\end{bmatrix}
$$

We can observe that the admittance matrix is symmetric which is, in fact, the sub-bloc that will be repeated for bigger admittance matrices. And we finally have

19

$$
\begin{bmatrix} \bar{I}_1 \\ \bar{I}_2 \\ \bar{I}_3 \\ \bar{I}_4 \\ \bar{I}_5 \end{bmatrix} = \begin{bmatrix} Y_{11} & Y_{21} & 0 & 0 & 0 \\ Y_{12} & Y_{22} & Y_{23} & Y_{24} & 0 \\ 0 & Y_{32} & Y_{33} & 0 & 0 \\ 0 & Y_{42} & 0 & Y_{44} & Y_{45} \\ 0 & 0 & 0 & Y_{54} & Y_{55} \end{bmatrix} \begin{bmatrix} \bar{V}_1 \\ \bar{V}_2 \\ \bar{V}_3 \\ \bar{V}_4 \\ \bar{V}_5 \end{bmatrix} \tag{3.10}
$$

## 1.3 The Power Flow Equations

**Mathematical Statement**

Let define the net complex power injection into a bus, we assume that all quantities are in per unit :

$$
\bar{S}_k = \bar{V}_k \bar{I}_k^* \tag{3.11}
$$

From the eq. (3.10), we can easily derive the current injection into any bus k :

$$
\bar{I}_k = \sum_{j=1}^{N} Y_{kj} \bar{V}_j \tag{3.12}
$$

Substitution of eq. (3.12) into eq. (3.11) yields

$$
\bar{S}_k = \bar{V}_k \left( \sum_{j=1}^{N} Y_{kj} \bar{V}_j \right)^* \tag{3.13}
$$

One can develop the eq. (3.13) since $V$ is a phasor and the admittance $Y_{kj}$ is a complex number

$$
\begin{aligned}
\bar{S}_k = \bar{V}_k \sum_{j=1}^{N} Y_{kj}^* \bar{V}_j^* &= |V_k| \angle \theta_k \sum_{j=1}^{N} (G_{kj} + jB_{kj})^* (|V_j| \angle \theta_j)^* \\
&= \sum_{j=1}^{N} |V_k||V_j| \angle (\theta_k - \theta_j)(G_{kj} - jB_{kj}) \tag{3.14}
\end{aligned}
$$

From the Euler relation, we can express the phasor relation as a complex function of sine, $|V|\angle\theta = |V|(cos\theta + jsin\theta)$. Eq. (3.14) is rewriting as follow

$$\bar{S}_k = \sum_{j=1}^{N} |V_k||V_j|(cos(\theta_k - \theta_j) + jsin(\theta_k - \theta_j))(G_{kj} - jB_{kj}) \tag{3.15}$$

Recall that $\bar{S}_k = P_k + jQ_k$, so we end up with two equations, one for the real part and one for the imaginary part.

$$\begin{cases} P_k = \sum_{j=1}^{N} |V_k||V_j|(G_{kj}cos(\theta_k - \theta_j) + B_{kj}sin(\theta_k - \theta_j)) \\ Q_k = \sum_{j=1}^{N} |V_k||V_j|(G_{kj}sin(\theta_k - \theta_j) - B_{kj}cos(\theta_k - \theta_j)) \end{cases} \tag{3.16}$$

**Analytic statement of the power flow problem**

Assume that we have a network with N buses. Among these, $N_G$ are voltage-regulating buses, more precisely these are generators. One of these latter is taken as the slack bus, usually the first bus, its phase angle and voltage magnitude are fixed, usually $|V| = 1pu$ and $\theta = 0$. Thus there are $N_{PV} = N_G - 1$ buses that we call PV buses and $N_{PQ} = N - N_G$ buses that we call PQ buses.

We can recall the two eq. (3.16) of above with the appropriate number of equations at stake.

$$\begin{cases} P_k = \sum_{j=1}^{N} |V_k||V_j|(G_{kj}cos(\theta_k - \theta_j) + B_{kj}sin(\theta_k - \theta_j)), & k = 2, ..., N \\ Q_k = \sum_{j=1}^{N} |V_k||V_j|(G_{kj}sin(\theta_k - \theta_j) - B_{kj}cos(\theta_k - \theta_j)), & k = N_{PV} + 2, ..., N \end{cases} \tag{3.17}$$

The purpose of the power flow problem is to find the phase angle at all buses except at the slack bus, i.e., $\theta_k$ $\forall$ k=2,...,N and also to find the voltage magnitude at all PQ buses, i.e., $|V_k|$ $\forall$ k=$N_G$+1,...,N.

So we have N-1 phase angle unknowns and N-$N_{PV}$+1 voltage magnitude unknowns, which represent finally 2N-$N_{PV}$ unknowns. We can highlight, by looking at the system of eq. (3.17), that the $G_{kj}$ and $B_{jk}$ are part of the information given by the network that we study, i.e., the Y matrix. We can also see that the number of power injections is the same as the number of unknowns, so we have a system with 2N-$N_{PV}$ equations for 2N-$N_{PV}$ unknowns.

We can define the state vector which is the unknowns vector.

$$\underline{x} = \begin{bmatrix} \underline{\theta} \\ |\underline{V}| \end{bmatrix} = \begin{bmatrix} \theta_2 \\ \theta_2 \\ \vdots \\ \theta_N \\ |V_{N_{PV}+2}| \\ |V_{N_{PV}+3}| \\ \vdots \\ |V_N| \end{bmatrix} = \begin{bmatrix} x_1 \\ x_2 \\ \vdots \\ x_{N-1} \\ x_N \\ x_{N+1} \\ \vdots \\ x_{2N-N_{PV}} \end{bmatrix} \qquad (3.18)$$

We can also define the mismatch vector.

$$\underline{f}(\underline{x}) = \begin{bmatrix} f_1(\underline{x}) \\ \vdots \\ f_{N-1}(\underline{x}) \\ \overline{f_N(\underline{x})} \\ \vdots \\ f_{2N-N_{PV}}(\underline{x}) \end{bmatrix} = \begin{bmatrix} P_2(\underline{x}) - P_2 \\ \vdots \\ P_N(\underline{x}) - P_N \\ \overline{Q_{N_{PV}}(\underline{x}) - Q_{N_{PV}}} \\ \vdots \\ Q_N(\underline{x}) - Q_N \end{bmatrix} = \begin{bmatrix} \Delta P_2 \\ \vdots \\ \Delta P_N \\ \overline{\Delta Q_{N_{PV}}} \\ \vdots \\ \Delta Q_N \end{bmatrix} = \underline{0} \qquad (3.19)$$

This vector is used during the Newton-Raphson procedure to compute $\Delta \underline{x}$, seen in the "The Newton-Raphson Procedure" section. In fact, we never reach a pure zero but once we reach the defined error such that $| f(\underline{x}) | \leq \epsilon$, we can stop the procedure and the convergence is achieved.

## 1.4   Application of NR to Power Flow Problem

As developed in the "The Newton-Raphson Procedure" section, we can update the solution as follow :

$$\underline{x}^{(i+1)} = \underline{x}^{(i)} - \mathbf{J}^{-1}\underline{f}(\underline{x}^{(i)}) \qquad (3.20)$$

The key step of the procedure is to determine the Jacobian matrix $\mathbf{J}^{-1}$. Therefore, we can see from eq. (3.18) that we only have two sets of unknowns, the voltage magnitude and the phase angle.

Thus, the Jacobian will be composed of 4 sub-matrices since there are only four basic types of derivatives : $\underline{J}^{P\theta}$, $\underline{J}^{PV}$, $\underline{J}^{Q\theta}$, $\underline{J}^{QV}$. For the simplicity of the writing, the first superscript express the type of equation we differentiate while the second express the unknowns with respect to which we differentiate. So we can write,

$$\mathbf{J} = \begin{bmatrix} \underline{J}^{P\theta} & \underline{J}^{PV} \\ \underline{J}^{Q\theta} & \underline{J}^{QV} \end{bmatrix} \tag{3.21}$$

The update formula can be developed as follow

$$\mathbf{J}\Delta\underline{\mathbf{x}}^{(i)} = -\underline{\mathbf{f}}(\underline{\mathbf{x}}^{(i)})$$

$$\Leftrightarrow \begin{bmatrix} \underline{J}^{P\theta} & \underline{J}^{PV} \\ \underline{J}^{Q\theta} & \underline{J}^{QV} \end{bmatrix} \begin{bmatrix} \Delta\underline{\theta} \\ \Delta\underline{V} \end{bmatrix} = -\begin{bmatrix} \Delta\underline{P} \\ \Delta\underline{Q} \end{bmatrix} \tag{3.22}$$

We observe that

$$\begin{cases} \underline{J}^{P\theta}\Delta\underline{\theta} + \underline{J}^{PV}\Delta\underline{V} = -\Delta\underline{P} \\ \underline{J}^{Q\theta}\Delta\underline{\theta} + \underline{J}^{QV}\Delta\underline{V} = -\Delta\underline{Q} \end{cases} \tag{3.23}$$

The sub-matrices can be derived as following

For P-equations

$$\begin{cases} J^{P\theta}_{jk} = \dfrac{\partial P_j(\underline{x})}{\partial \theta_k} = |V_j||V_k|(G_{jk}sin(\theta_j - \theta_k) - B_{jk}cos(\theta_j - \theta_k)) \\[2mm] J^{P\theta}_{jj} = \dfrac{\partial P_j(\underline{x})}{\partial \theta_j} = -Q_j(\underline{x}) - B_{jj}|V_j|^2 \\[2mm] J^{PV}_{jk} = \dfrac{\partial P_j(\underline{x})}{\partial |V|_k} = |V_j||V_k|(G_{jk}cos(\theta_j - \theta_k) + B_{jk}sin(\theta_j - \theta_k)) \\[2mm] J^{PV}_{jj} = \dfrac{\partial P_j(\underline{x})}{\partial |V|_j} = \dfrac{P_j(\underline{x})}{|V|_j} + G_{jj}|V|_j \end{cases} \tag{3.24}$$

For Q-equations

$$\begin{cases} J^{Q\theta}_{jk} = \dfrac{\partial Q_j(\underline{x})}{\partial \theta_k} = -|V_j||V_k|(G_{jk}cos(\theta_j - \theta_k) + B_{jk}sin(\theta_j - \theta_k)) \\[2mm] J^{Q\theta}_{jj} = \dfrac{\partial Q_j(\underline{x})}{\partial \theta_j} = P_j(\underline{x}) - G_{jj}|V|^2_j \\[2mm] J^{QV}_{jk} = \dfrac{\partial Q_j(\underline{x})}{\partial |V|_k} = |V_j|(G_{jk}sin(\theta_j - \theta_k) - B_{jk}cos(\theta_j - \theta_k)) \\[2mm] J^{QV}_{jj} = \dfrac{\partial Q_j(\underline{x})}{\partial |V|_j} = \dfrac{Q_j(\underline{x})}{|V|_j} - B_{jj}|V|_j \end{cases} \tag{3.25}$$

The application of the Newton-Raphson procedure to the power flow problem has been mathematically

developed. Let now derive the numerical procedure to perform a sensitivity analysis.

# 2 Sensitivity Analysis [7]

Secure a load means to constantly supply them. As one knows the NO-BREAK KS® can provide this service. Another important feature that this UPS system can support is a voltage regulation at the bus load.

In conditioning mode, the network bus voltage is steadily at 1 pu. The only manner to control the voltage at the bus load is to change the excitation of the UPS system. The latter acts as a synchronous condenser.

Numerically, instead of calibrate the load voltage by try-and-error method, one can use the sensitivity analysis to directly know how the output voltage of the UPS system influences the load voltage.

The sensitivity analysis which will be developed in this chapter requires in advance to define the equations and their notations used. It is the subject of the next section.

## 2.1 Derivation of the Control Model

As developed in Section 1.3, generators are represented as PV buses with adjustable parameters such as active power $P_{Gi}$ and terminal voltage $V_{Gi}$. Load buses are known as PQ buses where active power $P_{Di}$ and reactive power $Q_{Di}$ are specified. Let denote PQ-bus voltages $V_D$ and $\theta_D$, PV-bus voltages $V_G$ and $\theta_G$ and active power $P_G$.

The unknown vector $\underline{x}$ and generator vector $\underline{y}$ are respectively :

$$\underline{x} = \begin{bmatrix} \theta_D \\ \theta_G \\ V_D \end{bmatrix}, \underline{y} = \begin{bmatrix} V_{slack} \\ V_G \\ P_G \end{bmatrix}$$

The system power equations of PQ-bus and PV-bus are :

$$\begin{cases} g_{PDi} = P_{Di}^S - \sum_{j=1}^{N} |V_k||V_j|(G_{kj}cos(\theta_k - \theta_j) + B_{kj}sin(\theta_k - \theta_j)) = 0 \\ g_{QDi} = Q_{Di}^S - \sum_{j=1}^{N} |V_k||V_j|(G_{kj}sin(\theta_k - \theta_j) - B_{kj}cos(\theta_k - \theta_j)) = 0 \\ g_{PGi} = P_{Gi}^S - \sum_{j=1}^{N} |V_k||V_j|(G_{kj}cos(\theta_k - \theta_j) + B_{kj}sin(\theta_k - \theta_j)) = 0 \end{cases} \quad (3.26)$$

Consequently, we can clearly introduce the theoretical basis of the sensitivity analysis.

## 2.2 Sensitivity of Generation Variable to Load Voltage Variable

The objective is to know the sensitivity of the generation voltage variable to the load voltage variable. Indeed, once the sensitivity matrix is known, one can easily tune the terminal voltage of the NO-BREAK KS to regulate their downstream load.

Total differential for Formula (3.26) implicit's function equation is

$$dg = \frac{\partial g}{\partial x}dx + \frac{\partial g}{\partial y}dy = 0 \tag{3.27}$$

Where

$$dx = \begin{bmatrix} d\theta_2 \\ \vdots \\ d\theta_N \\ dV_2 \\ \vdots \\ dV_{N-N_{PV}} \end{bmatrix}, dy = \begin{bmatrix} dV_{G1} \\ \vdots \\ dV_{GN_G} \\ dP_{G1} \\ \vdots \\ dP_{GN_G} \end{bmatrix}$$

The rate of change of g to x, $\frac{\partial g}{\partial x}$, was derived in Section 1.1. In other word, this is the so called Jacobian matrix. Formula (3.27) can easily be written in matrix form

$$\mathbf{J} \begin{bmatrix} d\theta_2 \\ \vdots \\ d\theta_N \\ dV_2 \\ \vdots \\ dV_{N-N_{PV}} \end{bmatrix} = - \begin{bmatrix} \sum_{i \in N_G} \frac{\partial g_{PD1}}{\partial V_{Gi}} dV_{Gi} \\ \vdots \\ \sum_{i \in N_G} \frac{\partial g_{PD_{N-N_{PV}}}}{\partial V_{Gi}} dV_{Gi} \\ dP_{G1} + \frac{\partial P_{G1}}{\partial V_{G1}} dV_{G1} \\ \vdots \\ dP_{GN_G} + \frac{\partial P_{GN_G}}{\partial V_{GN_G}} dV_{GN_G} \\ \sum_{i \in N_G} \frac{\partial g_{QD1}}{\partial V_{Gi}} dV_{Gi} \\ \vdots \\ \sum_{i \in N_G} \frac{\partial g_{PQ_{N-N_{PV}}}}{\partial V_{Gi}} dV_{Gi} \end{bmatrix} \tag{3.28}$$

An iterative loop is required in order to find the response of the load voltage magnitude due to a unit change of the generation terminal voltage of each NO-BREAK KS. That is to say, setting $dy_i = 1$, $dy_j = 0$

(i=1,2,...,$2N_{PV}+1$, j≠i) and then solving successively $dx_i$. In matrix form

$$\mathbf{J}d\underline{x}_i = -\frac{\partial g}{\partial \underline{y}}\begin{bmatrix} 0 \\ \vdots \\ 1 \\ \vdots \\ 0 \end{bmatrix} \tag{3.29}$$

One can denote **D**, the rate of change of $\underline{x}$ to $\underline{y}$ or $\mathbf{D} = \mathbf{J}^{-1}\frac{\partial g}{\partial \underline{y}}$. Once this matrix is obtained, one can easily find the rate of change of a particular load voltage to the terminal voltage of one NO-BREAK KS® . Therefore, the differential equation is

$$d\underline{x} = \mathbf{D}d\underline{y} \tag{3.30}$$

Finally, for this application, the system of equations to be solved is

$$\begin{bmatrix} dV_{G1} \\ \vdots \\ dV_{GN_G} \end{bmatrix} = \begin{bmatrix} \frac{\partial V_{G1}}{\partial V_{PD1}} & \cdots & \frac{\partial V_{G1}}{\partial V_{PDN-N_{PV}}} \\ \vdots & \ddots & \vdots \\ \frac{\partial V_{GN_G}}{\partial V_{PD1}} & \cdots & \frac{\partial V_{GN_G}}{\partial V_{PDN-N_{PV}}} \end{bmatrix} \begin{bmatrix} dV_{PD1} \\ \vdots \\ dV_{PDN-N_{PV}} \end{bmatrix} \tag{3.31}$$

# 3 Fault Study [8]

In this chapter, the techniques used to compute the voltages of different buses, during the fault, will be derived. In order to determine the magnitude of the short-circuit current which will be a crucial information for the dimensioning of the circuit breakers and the adjustment of the protections settings.

The fault study is divided into two main parts : the analysis of balanced faults and the analysis of unbalanced faults.

## 3.1 Analysis of Balanced Faults

The balanced faults are encountered when there is a symmetrical three-phase short-circuit in the network. In other words, the per phase analysis is still applicable.

**Three-phase Short-circuits**

Let consider an IP topology with N buses. Each DRUPS is represented by a Thévenin equivalent as can be seen in Figure 3.2.
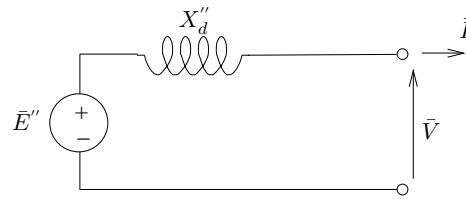


Figure 3.2: Equivalent Circuit of a DRUPS

The electromotive force $E''$ is constant during the first moments of the short-circuit, indeed, the latter is proportional to the flux of the field windings which is unchanged during the first moments.

Each load is supposed to behave as a constant admittance which is also a correct hypothesis during the first moments of the short-circuit. The equivalent admittance $Y_c$ of each load can be computed using the pre-fault active and reactive power consumed by it and the voltage at its terminal. One have

$$Y_C = \frac{P(0^-) - jQ(0^-)}{[\bar{V}(0^-)]^2} \tag{3.32}$$

Let now suppose that node f is subjected to a short-circuit with impedance $Z_f$. The voltage-current equation of node f is

$$\bar{V}_f = Z_f \bar{I}_f \tag{3.33}$$

In the case of a "solid" fault, $Z_f$ is null.

The network when bus f undergoes a short-circuit is shown in Figure 3.3 and for simplicity of computation, the DRUPS are represented by their Norton equivalent.

27
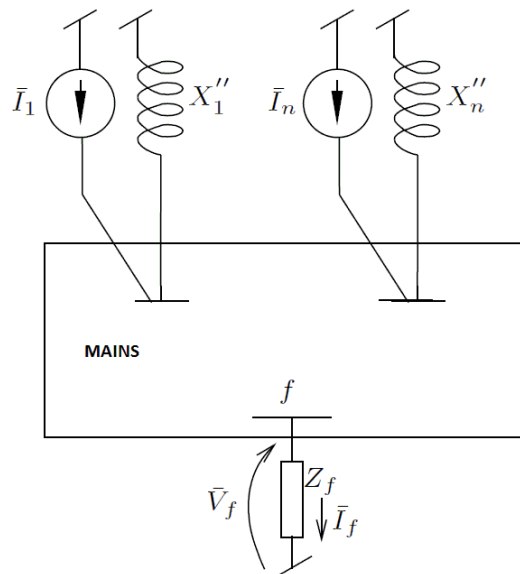
Figure 3.3: Short-Circuit on bus f

The network equations are :

$$\bar{\mathbf{I}} = \mathbf{Y}\bar{\mathbf{V}} \tag{3.34}$$

Where

- $\bar{\mathbf{I}}$ is the vector of complex currents injected in the N buses
- $\bar{\mathbf{V}}$ is the vector of complex voltages at the N buses
- $\mathbf{Y}$ is bus admittance matrix

The derivation of the bus admittance matrix has been developed in Section 1.2. Although, it remains to add $\frac{1}{jX''}$ to the DRUPS buses and $Y_c$ to the load buses. One can notice that the default impedance $Z_f$ is not included in the $\mathbf{Y}$ matrix. One could add $Y_f = \frac{1}{Z_f}$ to the right diagonal term in the matrix but two practical drawbacks are encountered:

- For each new faults in the network, one need to modify $\mathbf{Y}$ by adding $Y_f$
- A "solid" is theoretically represented by a null impedance so $Y_f$ would be infinite

The following derivation does not require to add $Y_f$ in the $\mathbf{Y}$ matrix and thus allows to work with the $\mathbf{Y}$ matrix before the fault. The computation of the during-fault voltages is done by a superposition method.

Under the effect of the currents $\bar{I}_1, \bar{I}_2, ..., \bar{I}_n$ injected by the DRUPS and the current $\bar{I}_f$ drawn at bus f, the eq. (3.34) can be decomposed such that :

$$\mathbf{Y}\bar{\mathbf{V}} = \begin{bmatrix} \bar{I}_1 \\ \bar{I}_2 \\ \vdots \\ \bar{I}_n \\ 0 \\ \vdots \\ \vdots \\ 0 \end{bmatrix} + \begin{bmatrix} 0 \\ \vdots \\ \vdots \\ 0 \\ -\bar{I}_f \\ 0 \\ \vdots \\ 0 \end{bmatrix} \tag{3.35}$$

By superposition, the solution $\bar{\mathbf{V}}$ is the sum of two terms :

$$\bar{\mathbf{V}} = \bar{\mathbf{V}}(0^-) + \Delta\bar{\mathbf{V}} \tag{3.36}$$

With

$$\mathbf{Y}\bar{\mathbf{V}}(0^-) = \begin{bmatrix} \bar{I}_1 \\ \bar{I}_2 \\ \vdots \\ \bar{I}_n \\ 0 \\ \vdots \\ \vdots \\ 0 \end{bmatrix} \tag{3.37}$$

And

$$\mathbf{Y}\Delta\bar{\mathbf{V}} = -\bar{I}_f \begin{bmatrix} 0 \\ \vdots \\ \vdots \\ 0 \\ 1 \\ 0 \\ \vdots \\ 0 \end{bmatrix} = -\bar{I}_f \mathbf{e}_f \tag{3.38}$$

$\bar{\mathbf{V}}(0^-)$ is the vector of bus voltages before the fault occurs in the system. $\Delta\bar{\mathbf{V}}$ can be consider as a correction which simulate the effect of the short-circuit. And $\mathbf{e}_f$ is a vector of zeros except for the f-th one which is equal to 1.

At this point, the value of $\bar{I}_f$ is still unknown. So, let one solves the linear system :

$$\mathbf{Y}\,\Delta\bar{\mathbf{V}}^{(1)} = \mathbf{e}_f \tag{3.39}$$

The right hand side of eq. (3.38) and (3.39) differs by the factor $-\bar{I}_f$, one has :

$$\Delta\bar{\mathbf{V}} = -\bar{I}_f\Delta\bar{\mathbf{V}}^{(1)} \tag{3.40}$$

Introducing this result in eq. (3.36), one obtains :

$$\bar{\mathbf{V}} = \bar{\mathbf{V}}(0^-) - \bar{I}_f\Delta\bar{\mathbf{V}}^{(1)} \tag{3.41}$$

The f-th component of this equation is

$$\bar{V}_f = \bar{V}_f(0^-) - \bar{I}_f\Delta\bar{V}_f^{(1)} \tag{3.42}$$

By combining the above equation and eq.(3.33), one obtains the value of $\bar{I}_f$ :

$$\bar{I}_f = \frac{\bar{V}_f(0^-)}{\Delta\bar{V}_f^{(1)} + Z_f} \tag{3.43}$$

And finally, by injecting this solution in eq.(3.41), one finds the post-fault bus voltages

$$\bar{\mathbf{V}} = \bar{\mathbf{V}}(0^-) - \frac{\bar{V}_f(0^-)}{\Delta\bar{V}_f^{(1)} + Z_f}\Delta\bar{\mathbf{V}}^{(1)} \tag{3.44}$$

To complete the analysis of the fault study, it remains to develop the second part concerning the analysis of unbalanced faults.

## 3.2  Analysis of Unbalanced Faults

For the analysis of unbalanced faults, two approaches can be used.

The first approach is a "traditional" approach whose purpose is to solve three balanced systems : the positive-sequence system, the negative-sequence system and the zero-sequence system. According to the network topology, one assembles the positive-sequence models, the negative-sequence models and the zero-sequence models taking into account the components of this network such that lines, transformers, loads and generators. At the location of the fault, one connects the positive-, negative- and zero-sequence models in a way that the nature of the fault is taking into account. Once the voltages and currents are found, one can easily use the Fortescue transformation and obtains the solution in (a,b,c).

The second approach, used in this master thesis, is based on the resolution of the equation system in (a,b,c) :

$$\bar{\mathbf{I}} = \mathbf{Y}\bar{\mathbf{V}} \tag{3.45}$$

Let consider a N-bus network. The bus admittance matrix $\mathbf{Y}$ is thus a $3N$x$3N$ matrix and the vector of three-phase injected currents $\bar{\mathbf{I}}$ is a $3N$x$1$ size vector. These latter can be constructed by assembling individual models that represent the loads, mains, DRUPS, lines and transformers according to the network topology. One must highlight that some of the models needs values from an initial power flow computation of the balanced system.

Let us clarify successively the different models.

**Load Model**

Firstly, the model of a star-connected load will be developed. And secondly, the model of a delta-connected load will be developed.

Figure 3.4 shows a star-connected load. As mentioned, one needs some values from an initial power flow computation such as the complex power consumed in one phase $P + jQ$ and the magnitude of the phase-to-neutral voltage under which this power is consumed $V$. The admittance $y$ can be deduced :

$$y = \frac{P - jQ}{V^2} \tag{3.46}$$
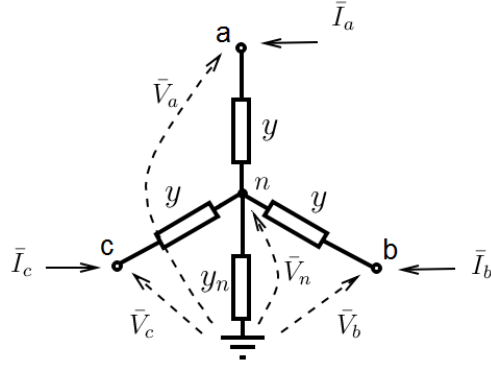
Figure 3.4: Star-Connected Load

By Ohm's law,

$$
\begin{cases}
\bar{I}_a = y(\bar{V}_a - \bar{V}_n) & \text{(3.47a)} \\
\bar{I}_b = y(\bar{V}_b - \bar{V}_n) & \text{(3.47b)} \\
\bar{I}_c = y(\bar{V}_c - \bar{V}_n) & \text{(3.47c)} \\
\bar{I}_a + \bar{I}_b + \bar{I}_c = yn\bar{V}_n & \text{(3.47d)}
\end{cases}
$$

By adding eq. (3.47a, 3.47b and 3.47c) and introducing the result in eq.(3.47d) yields :

$$
\bar{V}_n = \frac{y\bar{V}_a + y\bar{V}_b + y\bar{V}_c}{y_{tot}} \tag{3.48}
$$

With $y_{tot} = 3y + y_n$.

Injecting eq. (3.48) into eq. (3.47a, 3.47b and 3.47c) and arranging the results in matrix form gives :

$$
\begin{bmatrix} \bar{I}_a \\ \bar{I}_b \\ \bar{I}_c \end{bmatrix} =
\underbrace{\begin{bmatrix}
y - \dfrac{y^2}{y_{tot}} & -\dfrac{y^2}{y_{tot}} & -\dfrac{y^2}{y_{tot}} \\
-\dfrac{y^2}{y_{tot}} & y - \dfrac{y^2}{y_{tot}} & -\dfrac{y^2}{y_{tot}} \\
-\dfrac{y^2}{y_{tot}} & -\dfrac{y^2}{y_{tot}} & y - \dfrac{y^2}{y_{tot}}
\end{bmatrix}}_{\text{Contribution to matrix } \mathbf{Y}}
\begin{bmatrix} \bar{V}_a \\ \bar{V}_b \\ \bar{V}_c \end{bmatrix} \tag{3.49}
$$

Let derive the delta-connected load model. Figure 3.5 shows a delta-connected load. The complex power $P + jQ$ consumed by the load needs also to be know and the magnitude of the phase-to-phase voltage $U$ under which this power is consumed is also obtained by an initial power flow computation.
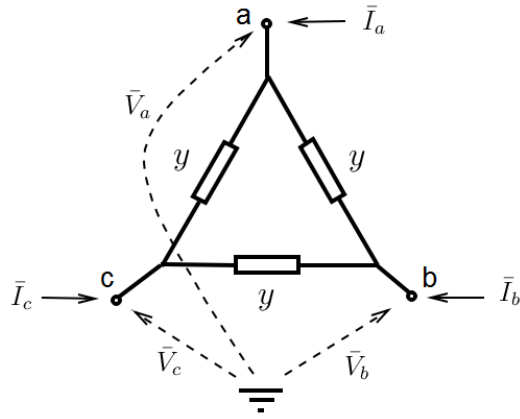
Figure 3.5: Delta-Connected Load

The branch admittance is given by :

$$y = \frac{P - jQ}{U^2} \tag{3.50}$$

By Ohm's law,

$$
\begin{cases}
\bar{I}_a = y(\bar{V}_a - \bar{V}_b) + y(\bar{V}_a - \bar{V}_c) & \text{(3.51a)} \\
\bar{I}_b = y(\bar{V}_b - \bar{V}_a) + y(\bar{V}_b - \bar{V}_c) & \text{(3.51b)} \\
\bar{I}_c = y(\bar{V}_c - \bar{V}_a) + y(\bar{V}_c - \bar{V}_b) & \text{(3.51c)}
\end{cases}
$$

The system of eq. (3.51) can be written in matrix form :

$$
\begin{bmatrix} \bar{I}_a \\ \bar{I}_b \\ \bar{I}_c \end{bmatrix} = \underbrace{\begin{bmatrix} 2y & -y & -y \\ -y & 2y & -y \\ -y & -y & 2y \end{bmatrix}}_{\text{Contribution to matrix } \mathbf{Y}} \begin{bmatrix} \bar{V}_a \\ \bar{V}_b \\ \bar{V}_c \end{bmatrix} \tag{3.52}
$$

**Model of Balanced Norton Equivalent Of The Mains**

As can be seen in Figure 3.2, the mains is modeled as a three-phase Norton equivalent which is suitable for the present application. Despite the fact that the mains could also be represented by a three-phase Thévenin equivalent as seen in Figure 3.6.

For this model, one needs to know the complex power produced by one phase $P + jQ$, the Thevenin

33
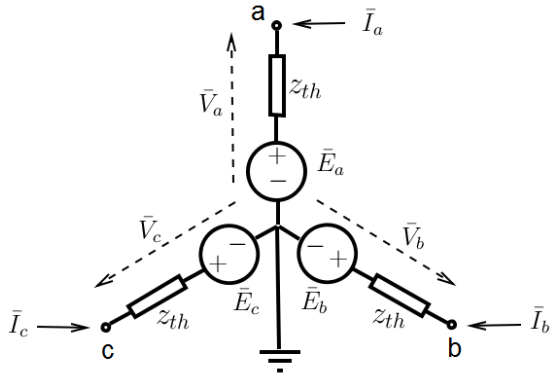
Figure 3.6: Voltages and Impedances
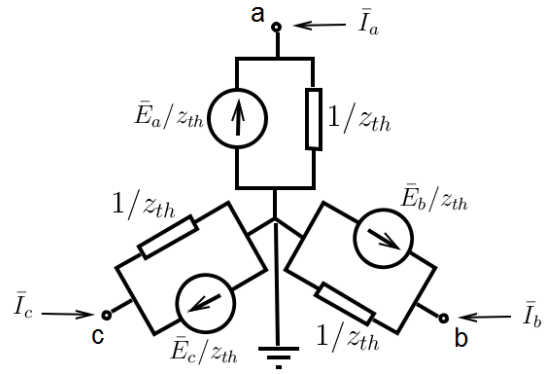


Figure 3.7: Currents and Admittances

impedance $z_{th} = \frac{1}{S_{sc}}$ where $S_{sc}$ is the short-circuit power and the complex (phase-to-neutral) voltage of phase a $\bar{V}_a$. The electromotive force of each phase depends of these physical quantities :

$$
\begin{cases}
\bar{E}_a = \bar{V}_a + z_{th}\dfrac{P - jQ}{\bar{V}_a^*} & \text{(3.53a)} \\[2mm]
\bar{E}_b = a^2\bar{E}_a & \text{(3.53b)} \\[2mm]
\bar{E}_c = a\bar{E}_a & \text{(3.53c)}
\end{cases}
$$

Where a $= e^{j\frac{2\pi}{3}}$.

By Ohm's law,

$$
\begin{cases}
\bar{I}_a = \dfrac{(\bar{V}_a - \bar{E}_a)}{z_{th}} & \text{(3.54a)} \\[3mm]
\bar{I}_b = \dfrac{(\bar{V}_b - \bar{E}_b)}{z_{th}} & \text{(3.54b)} \\[3mm]
\bar{I}_c = \dfrac{(\bar{V}_c - \bar{E}_c)}{z_{th}} & \text{(3.54c)}
\end{cases}
$$

The matrix form of this system of equations yields :

$$
\begin{bmatrix} \bar{I}_a \\ \bar{I}_b \\ \bar{I}_c \end{bmatrix} = \underbrace{\begin{bmatrix} \frac{1}{z_{th}} & 0 & 0 \\ 0 & \frac{1}{z_{th}} & 0 \\ 0 & 0 & \frac{1}{z_{th}} \end{bmatrix}}_{\text{Contribution to matrix } \mathbf{Y}} \begin{bmatrix} \bar{V}_a \\ \bar{V}_b \\ \bar{V}_c \end{bmatrix} - \underbrace{\begin{bmatrix} \bar{E}_a/z_{th} \\ \bar{E}_b/z_{th} \\ \bar{E}_c/z_{th} \end{bmatrix}}_{\text{Contribution to matrix } \bar{I}} \tag{3.55}
$$

34

**DRUPS Model**

For the generator model shown in Figure 3.8, the contribution to admittance matrix $\mathbf{Y}$ can be derived from the positive, negative and zero-sequence equivalent circuits of a synchronous generator.
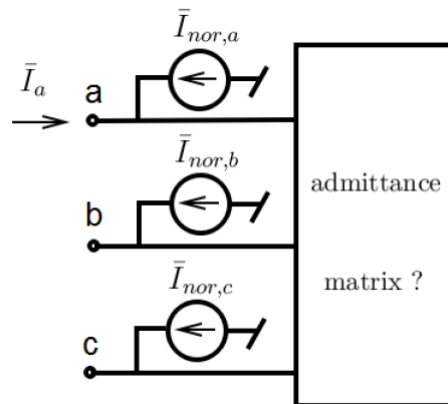


Figure 3.8: Generator model

Let assume a star configuration, with an impedance $z_n$ in the neutral. The positive-, negative- and zero-sequence equivalent circuits of a synchronous generator are shown in Figure 3.9.



positive sequence     negative sequence     zero sequence
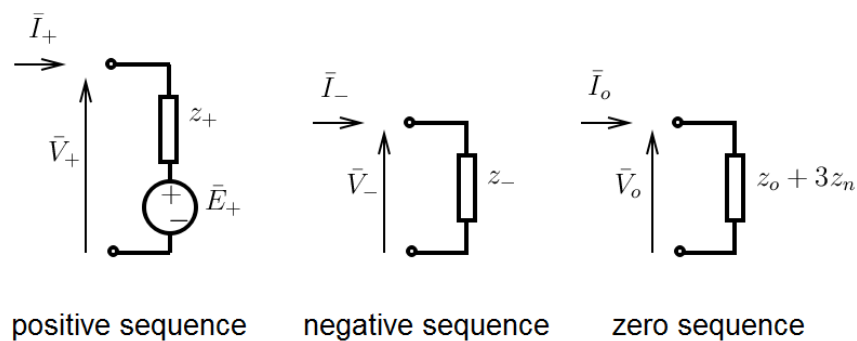
Figure 3.9: Symmetrical Components Circuits of a Synchronous Generator

The equivalent admittance matrix $\mathbf{Y}_G$ of the synchronous generator can easily be derived from positive-, negative- and zero-sequence impedances of the latter. Indeed, using the inverse Fortescue Transformation yields :

$$\mathbf{Y}_G = \mathbf{T}\mathbf{Y}_F\mathbf{T}^{-1} \tag{3.56}$$

With:

$$\mathbf{Y}_F = \begin{bmatrix} \frac{1}{z_+} & 0 & 0 \\ 0 & \frac{1}{z_+} & 0 \\ 0 & 0 & \frac{1}{z_0+3z_n} \end{bmatrix} \text{ and } \mathbf{T} = \begin{bmatrix} 1 & 1 & 1 \\ a^2 & a & 1 \\ a & a^2 & 1 \end{bmatrix}$$

The contribution to admittance matrix $\mathbf{Y}$ has been derived, it only remains to derive the contribution to the currents vector $\bar{\mathbf{I}}$. For that, one need to identify $\bar{I}_{nor,a}$, $\bar{I}_{nor,b}$ and $\bar{I}_{nor,c}$ by assuming an initial balanced operating conditions. For the voltages:

$$\begin{cases} \bar{V}_+ = \bar{V}_a & (3.57a) \\ \bar{V}_- = 0 & (3.57b) \\ \bar{V}_0 = 0 & (3.57c) \end{cases}$$

For the currents:

$$\begin{cases} \bar{I}_+ = \bar{I}_a = -\dfrac{P - jQ}{\bar{V}_a^*} & (3.58a) \\ \bar{I}_- = 0 & (3.58b) \\ \bar{I}_0 = 0 & (3.58c) \end{cases}$$

Hence,

$$\bar{E}_+ = \bar{V}_+ - z_+\bar{I}_+ = \bar{V}_a + z_+ \frac{P - jQ}{\bar{V}_a^*} \tag{3.59}$$

Thus, the contribution to vector $\bar{\mathbf{I}}$ is

$$\begin{bmatrix} \bar{I}_{nor,a} \\ \bar{I}_{nor,b} \\ \bar{I}_{nor,b} \end{bmatrix} = \begin{bmatrix} \bar{E}_+/z_+ \\ a^2\bar{E}_+/z_+ \\ a\bar{E}_+/z_+ \end{bmatrix}$$

**Line Model**

A line can be modeled as shunt capacitive parts and series resisitive-inductive parts as shown in Figure 3.10. The branches of the IP topology are only inductive which simplifies the derivation of the model.
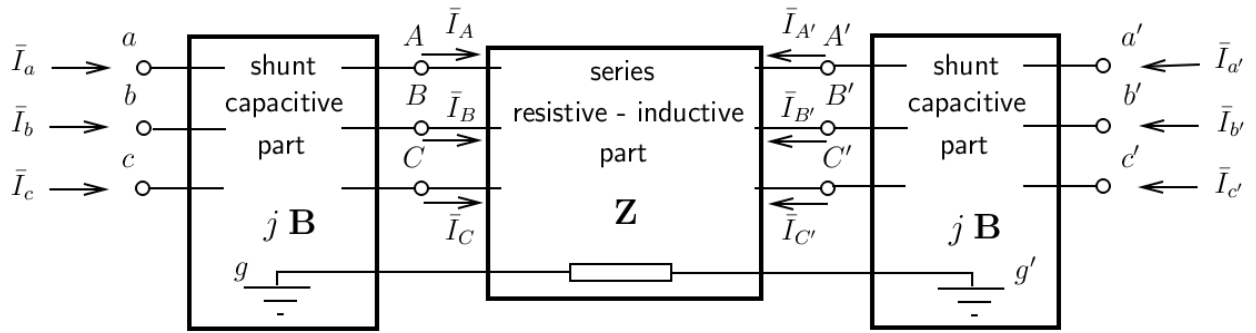
Figure 3.10: Line Model

The positive-sequence series impedance $z_+ = jx_+$ and the zero-sequence series impedance $z_0 = jx_0$ are the only data required for the derivation of the admittance matrix of the line $\mathbf{Y}_l$. Indeed, the voltage-current relations of the series part are

$$
\begin{bmatrix} \bar{V}_A - \bar{V}_g \\ \bar{V}_B - \bar{V}_g \\ \bar{V}_C - \bar{V}_g \end{bmatrix} = \mathbf{Z} \begin{bmatrix} \bar{I}_A \\ \bar{I}_B \\ \bar{I}_C \end{bmatrix} + \begin{bmatrix} \bar{V}_{A'} - \bar{V}_{g'} \\ \bar{V}_{B'} - \bar{V}_{g'} \\ \bar{V}_{C'} - \bar{V}_{g'} \end{bmatrix}
$$

$$
\Leftrightarrow \begin{bmatrix} \bar{I}_A \\ \bar{I}_B \\ \bar{I}_C \end{bmatrix} = \mathbf{Z}^{-1} \begin{bmatrix} \bar{V}_A - \bar{V}_g \\ \bar{V}_B - \bar{V}_g \\ \bar{V}_C - \bar{V}_g \end{bmatrix} - \mathbf{Z}^{-1} \begin{bmatrix} \bar{V}_{A'} - \bar{V}_{g'} \\ \bar{V}_{B'} - \bar{V}_{g'} \\ \bar{V}_{C'} - \bar{V}_{g'} \end{bmatrix}
$$

And

$$
\begin{bmatrix} \bar{I}_{A'} \\ \bar{I}_{A'} \\ \bar{I}_{A'} \end{bmatrix} = - \begin{bmatrix} \bar{I}_A \\ \bar{I}_B \\ \bar{I}_C \end{bmatrix}
$$

These results can be rewritten in matrix form :

$$
\begin{bmatrix} \bar{I}_A \\ \bar{I}_B \\ \bar{I}_C \\ \hline \bar{I}_{A'} \\ \bar{I}_{B'} \\ \bar{I}_{C'} \end{bmatrix} = \underbrace{\left[ \begin{array}{c|c} \mathbf{Z}^{-1} & -\mathbf{Z}^{-1} \\ \hline -\mathbf{Z}^{-1} & \mathbf{Z}^{-1} \end{array} \right]}_{\text{Contribution to matrix } \mathbf{Y}} \begin{bmatrix} \bar{V}_A - \bar{V}_g \\ \bar{V}_B - \bar{V}_g \\ \bar{V}_C - \bar{V}_g \\ \bar{V}_{A'} - \bar{V}_{g'} \\ \bar{V}_{B'} - \bar{V}_{g'} \\ \bar{V}_{C'} - \bar{V}_{g'} \end{bmatrix}
$$

37

**Transformer Model**

The admittance matrix of the transformer in (a,b,c) can be derive from the admittance matrix of the positive-, negative- and zero-sequence equivalent two-port. Figure 3.11 shows the transformer model.
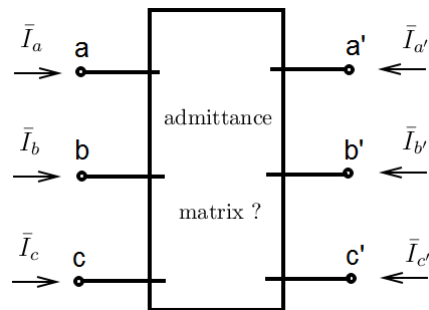


Figure 3.11: Transformer Model

The positive-equivalent circuit is shown in Figure 3.12. The goal is to determine the expression of the primary and secondary currents.
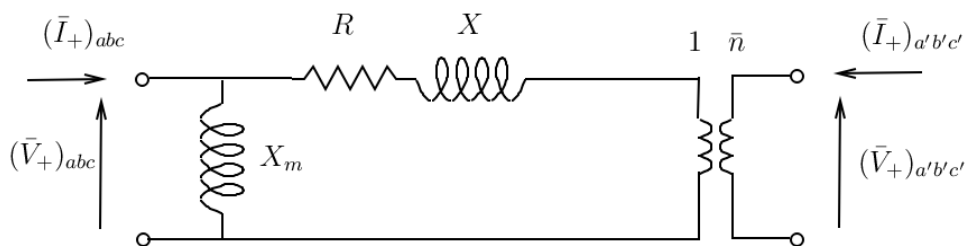


Figure 3.12: Positive-Sequence equivalent Circuit

By the theory of transformer and Ohm's law, one obtains :

$$
\begin{cases}
(\bar{I}_+)_{abc} = \dfrac{1}{jX_m}(\bar{V}_+)_{abc} + \dfrac{1}{R+jX}[(\bar{V}_+)_{abc} - \dfrac{1}{\bar{n}}(\bar{V}_+)_{a'b'c'}] & \text{(3.60a)} \\[2ex]
(\bar{I}_+)_{a'b'c'} = \dfrac{1}{\bar{n}^*}\dfrac{1}{R+jX}[(\bar{V}_+)_{a'b'c'} - (\bar{V}_+)_{abc}] & \text{(3.60b)}
\end{cases}
$$

Or in matrix form :

$$\begin{bmatrix} (\bar{I}_+)_{abc} \\ (\bar{I}_+)_{a'b'c'} \end{bmatrix} = \underbrace{\begin{bmatrix} \frac{1}{jX_m} + \frac{1}{R+jX} & -\frac{1}{\bar{n}} \frac{1}{R+jX} \\ -\frac{1}{\bar{n}^*} \frac{1}{R+jX} & -\frac{1}{|\bar{n}|^2} \frac{1}{R+jX} \end{bmatrix}}_{pos.-seq.admittancematrix} \begin{bmatrix} (\bar{V}_+)_{abc} \\ (\bar{V}_+)_{a'b'c'} \end{bmatrix}$$

Concerning the derivation of the negative-sequence admittance matrix, it is similar to the positive-sequence. However, one must replace $\bar{n}$ by $\bar{n}^*$ in the positive-sequence admittance matrix. So one has :

$$\begin{bmatrix} (\bar{I}_-)_{abc} \\ (\bar{I}_-)_{a'b'c'} \end{bmatrix} = \underbrace{\begin{bmatrix} \frac{1}{jX_m} + \frac{1}{R+jX} & -\frac{1}{\bar{n}^*} \frac{1}{R+jX} \\ -\frac{1}{\bar{n}} \frac{1}{R+jX} & -\frac{1}{|\bar{n}|^2} \frac{1}{R+jX} \end{bmatrix}}_{neg.-seq.admittancematrix} \begin{bmatrix} (\bar{V}_-)_{abc} \\ (\bar{V}_-)_{a'b'c'} \end{bmatrix}$$

The admittance matrix of the zero-sequence equivalent two-port depends on the type of transformer.

For the transformer of type Ynd* shown in Figure 3.13, the zero-sequence current can only flow through the neutral impedance in the primary.
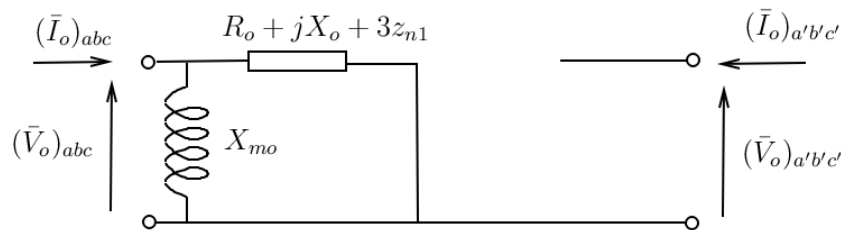


Figure 3.13: Zero-sequence Equivalent Two-port

The admittance matrix can easily be deduced from the above Figure :

$$\begin{bmatrix} (\bar{I}_o)_{abc} \\ (\bar{I}_o)_{a'b'c'} \end{bmatrix} = \underbrace{\begin{bmatrix} \frac{1}{jX_{mo}} + \frac{1}{R_0+jX_0+3z_{n1}} & 0 \\ 0 & 0 \end{bmatrix}}_{\text{zero-seq. admittance matrix}} \begin{bmatrix} (\bar{V}_o)_{abc} \\ (\bar{V}_o)_{a'b'c'} \end{bmatrix}$$

For the transformer of type YnYn0 as seen in Figure 3.14, the zero-sequence current can flow in both side of the transformer.

39
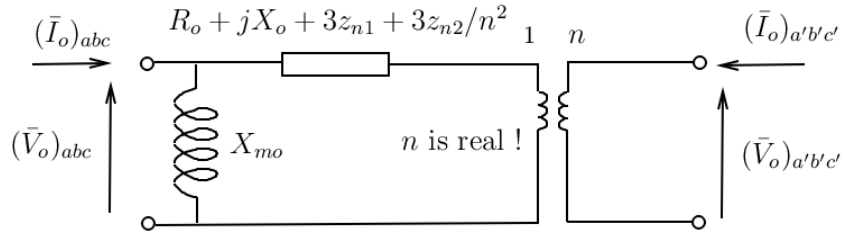
Figure 3.14: Zero-sequence Equivalent Two-port

The current-voltage relations are then :

$$
\begin{bmatrix} (\bar{I}_o)_{abc} \\ (\bar{I}_o)_{a'b'c'} \end{bmatrix} = \underbrace{\begin{bmatrix} \frac{1}{jX_{mo}} + \frac{1}{R_0+jX_0+3z_{n1}+3z_{n2}/n^2} & -\frac{1}{n}\frac{1}{R_0+jX_0+3z_{n1}+3z_{n2}/n^2} \\ -\frac{1}{n}\frac{1}{R_0+jX_0+3z_{n1}+3z_{n2}/n^2} & -\frac{1}{n^2}\frac{1}{R_0+jX_0+3z_{n1}+3z_{n2}/n^2} \end{bmatrix}}_{\text{zero-seq. admittance matrix}} \begin{bmatrix} (\bar{V}_o)_{abc} \\ (\bar{V}_o)_{a'b'c'} \end{bmatrix}
$$

And for a transformer of any other type, the zero-sequence can only flow through the magnetizing inductance as can be seen in Figure 3.15.
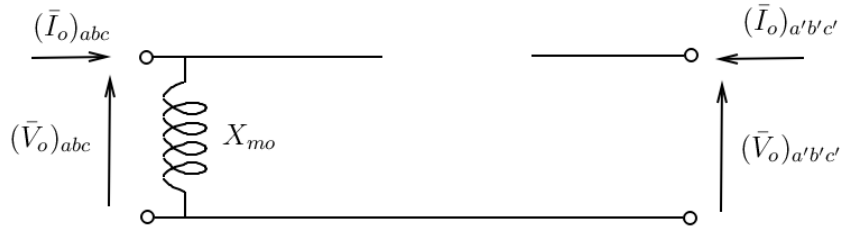


Figure 3.15: Zero-sequence Equivalent Two-port

The admittance matrix is easily derived :

$$
\begin{bmatrix} (\bar{I}_o)_{abc} \\ (\bar{I}_o)_{a'b'c'} \end{bmatrix} = \underbrace{\begin{bmatrix} \frac{1}{jX_{mo}} & 0 \\ 0 & 0 \end{bmatrix}}_{\text{zero-seq. admittance matrix}} \begin{bmatrix} (\bar{V}_o)_{abc} \\ (\bar{V}_o)_{a'b'c'} \end{bmatrix}
$$

One can now assemble the admittance matrices of all three sequences :

$$
\begin{bmatrix}
(\bar{I}_+)_{abc} \\
(\bar{I}_-)_{abc} \\
(\bar{I}_o)_{abc} \\
(\bar{I}_+)_{a'b'c'} \\
(\bar{I}_-)_{a'b'c'} \\
(\bar{I}_o)_{a'b'c'}
\end{bmatrix}
= \mathbf{Y}_F
\begin{bmatrix}
(\bar{V}_+)_{abc} \\
(\bar{V}_-)_{abc} \\
(\bar{V}_o)_{abc} \\
(\bar{V}_+)_{a'b'c'} \\
(\bar{V}_-)_{a'b'c'} \\
(\bar{V}_o)_{a'b'c'}
\end{bmatrix}
$$

With :

$$
\mathbf{Y}_F =
\begin{bmatrix}
\frac{1}{jX_m} + \frac{1}{R+jX} & 0 & 0 & -\frac{1}{\bar{n}}\frac{1}{R+jX} & 0 & 0 \\
0 & \frac{1}{jX_m} + \frac{1}{R+jX} & 0 & 0 & -\frac{1}{\bar{n}^*}\frac{1}{R+jX} & 0 \\
0 & 0 & y_{11} & 0 & 0 & y_{12} \\
-\frac{1}{\bar{n}^*}\frac{1}{R+jX} & 0 & 0 & -\frac{1}{|\bar{n}|^2}\frac{1}{R+jX} & 0 & 0 \\
0 & -\frac{1}{\bar{n}}\frac{1}{R+jX} & 0 & 0 & -\frac{1}{|\bar{n}|^2}\frac{1}{R+jX} & 0 \\
0 & 0 & y_{21} & 0 & 0 & y_{22}
\end{bmatrix}
$$

Where $\begin{bmatrix} y_{11} & y_{12} \\ y_{21} & y_{22} \end{bmatrix}$ depends on the type of transformer. One can use the inverse Fortescue transformation to obtain the contribution to admittance matrix $\mathbf{Y}$ :

$$
\begin{bmatrix}
\bar{I}_a \\
\bar{I}_b \\
\bar{I}_c \\
\bar{I}_{a'} \\
\bar{I}_{b'} \\
\bar{I}_{c'}
\end{bmatrix}
=
\underbrace{
\begin{bmatrix}
\mathbf{T} & \mathbf{0} \\
\mathbf{0} & \mathbf{T}
\end{bmatrix}
\mathbf{Y}_F
\begin{bmatrix}
\mathbf{T}^{-1} & \mathbf{0} \\
\mathbf{0} & \mathbf{T}^{-1}
\end{bmatrix}
}_{\text{Contribution to matrix } \mathbf{Y}}
\begin{bmatrix}
\bar{V}_a \\
\bar{V}_b \\
\bar{V}_c \\
\bar{V}'_a \\
\bar{V}'_b \\
\bar{V}'_c
\end{bmatrix}
$$

Let introduces the numerical techniques to take into account the three types of fault.

**Phase-to-ground Short-circuit**

For the simulation of a phase-to-ground short-circuit, one modifies the $\mathbf{Y}$ matrix such as phase i is connected to the ground by a small impedance :

$$y_{ii} = y_{ii} + y_f \tag{3.61}$$

Normally, $y_f$ should be infinite when it is a "solid" fault but for numerical reason, one takes, typically, $y_f = 10^6$.

**Phase-to-phase Short-circuit**

For the simulation of a short-circuit between two lines i and j, one modifies the **Y** as follow:

$$\begin{cases} y_{ii} = y_{ii} + y_f & \text{(3.62a)} \\ y_{ij} = y_{ij} - y_f & \text{(3.62b)} \\ y_{ji} = y_{ji} - y_f & \text{(3.62c)} \\ y_{jj} = y_{jj} + y_f & \text{(3.62d)} \end{cases}$$

**Two-phase-to-ground Short-circuit**

For the simulation of a short-circuit between two lines i and j and the ground, one modifies the **Y** as follow:

$$\begin{cases} y_{ii} = y_{ii} + y_f & \text{(3.63a)} \\ y_{jj} = y_{jj} + y_f & \text{(3.63b)} \end{cases}$$

We have just introduced the numerical tools for the power system analysis. Therefore, we can apply these developments in order to obtain numerical results.

# Chapter 4

# Numerical Simulations

This section will show the results of different numerical models that I developed using SCILAB.

Firstly, we will show the flowchart diagram of my program and explained the steps offer to the user in order to perform a case study.

Secondly, we will validate my developed numerical models in two steps. The first step, we use a topology for which circuits theory can easily find an analytical solution. Then we will compare the results of my program for this topology and we will find that the results are identical. The second step, concerning a complex problem, is to compare my results with these of a reference program used by the service of Prof. Thierry Van Cutsem, ARTERE.

At last, we will apply my program for the full study of a problem provided by EURO-DIESEL. And we will find that the results obtained by the technical service of EURO-DIESEL correspond with these found by my program.

## 1 Program Implementation

The flowchart of the program developed within the framework of this thesis is shown in Figure 4.1.

When the program is launched, one can choose between the conditioning mode or independent mode. Once the choice is made, the program automatically reads an Excel file where the topology data are stored and initializes the variables needed for the power flow problem. The user can solve the power flow problem for the normal stage which corresponds to the stage describes in the Excel file or skip it and directly goes to the fault study. If the user wants to solve the normal stage, the Newton-Raphson procedure is used until it converges and the sensitivity analysis is used in order to change the terminal voltage of the DRUPS to bring the load voltage to 1 per unit. Then another choice is proposed to the user to proceed a fault study or not, if the decides to skip this study then he is directly send to the choice of scenario. If the user wants a fault study, then the nature of short-circuit is proposed and depending on the nature, different script files are used to compute the post-fault voltages. And finally, the user can choose the scenario (loss of one DRUPS, loss

of two DRUPS or loss of distribution switchboard) to be perform and the program automatically writes the results in a text file.
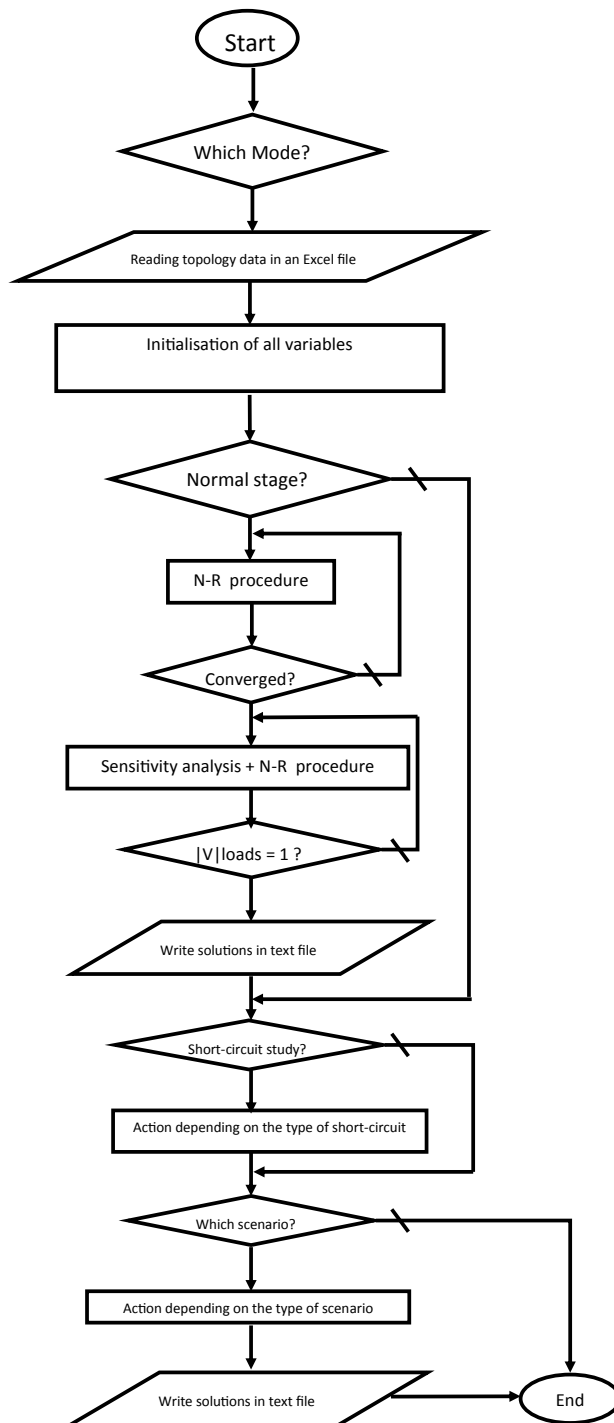


Figure 4.1: Flowchart of the Program

# 2 Validation

## 2.1 First validation test

First of all, the static model developed for EURO-DIESEL needs to be validate. For that, a test case is used. The latter is an IP star topology with two DRUPS as can be seen in Figure 4.2.
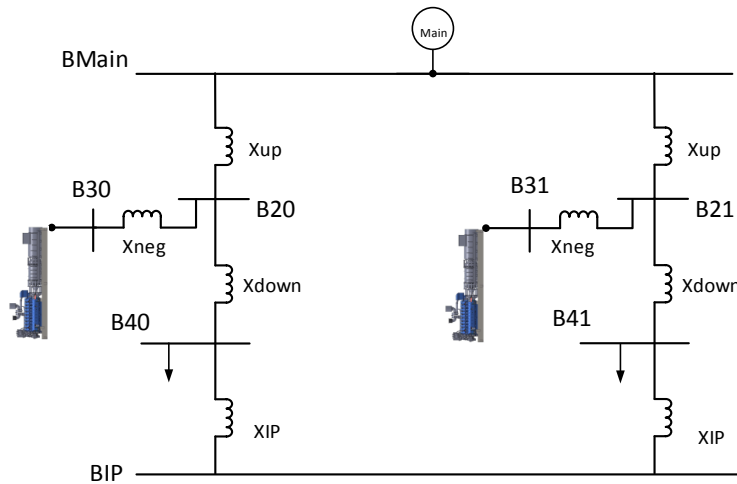


Figure 4.2: IP Star Topology with 2 DRUPS

The network topology data are given in the following Table

Table 4.1: Impedances of The Lines

|  | X[pu] |
|---|---|
| $X_{up}$ | 0.4008 |
| $X_{down}$ | 0.08016 |
| $X_{neg}$ | -0.0668 |
| $X_{IP}$ | 0.3 |

The origin of the negative value for the reactance $X_{neg}$ is explained in Annex A.

The particularity of this network is that the load at bus "B40" is 0 W and at bus "B41" is 500 kW. One expects that the ratio of the power flow coming from upstream and downstream of the load at "B41" will be exactly equal to the ratio of the upstream impedance's sum and the downstream impedance's sum. Mathematically, it gives

$$X_{upstream} = X_{up} + X_{down} = 0.4810 \tag{4.1}$$

$$X_{downstream} = X_{up} + X_{down} + 2X_{IP} = 1.081 \tag{4.2}$$

And the ratio between the eq. (4.1) and (4.2)

$$\frac{X_{upstream}}{X_{downstream}} = \frac{0.4810}{1.081} = 0.445 \tag{4.3}$$

The numerical power flow results are shown in the Table 4.2

Table 4.2: Voltage Profile

|          | $|V|$  | $\theta$  |
|----------|--------|-----------|
| $B_{Main}$ | 1.0000 | 0       |
| $B_{20}$ | 1.0001 | -0.0235 |
| $B_{30}$ | 0.9999 | -0.0235 |
| $B_{40}$ | 1.0000 | -0.0282 |
| $B_{21}$ | 1.0001 | -0.0528 |
| $B_{31}$ | 0.9997 | -0.0528 |
| $B_{41}$ | 1.0000 | -0.0634 |
| $B_{IP}$ | 0.9998 | -0.0458 |

One can compute the active power flowing through lines "$B_{IP}$-$B_{41}$" and "$B_{21}$-$B_{41}$".

$$P_{upstream} = \frac{|V_{B_{IP}}||V_{B_{41}}|sin(\theta_{B_{IP}} - \theta_{B_{41}})}{X_{IP}} = 153.9798 \ kW \tag{4.4}$$

$$P_{downstream} = \frac{|V_{B_{21}}||V_{B_{41}}|sin(\theta_{B_{21}} - \theta_{B_{41}})}{X_{down}} = 346.0202 \ kW \tag{4.5}$$

Finally the ratio between eq. (4.4) and (4.5) is

$$\frac{P_{upstream}}{P_{downstream}} = \frac{153.9798}{346.0202} = 0.445 \tag{4.6}$$

In conclusion, the ratio (eq. (69)) of the power flow coming from upstream and downstream of the load at "B41" is exactly equal to the ratio (eq. (66)) of the upstream impedance's sum and the downstream impedance's sum as expected.

## 2.2 Second validation test

The second test is carried out in order to prove that the solution displayed by the program developed for EURO-DIESEL is similar to the solution found by ARTERE for a complex problem.
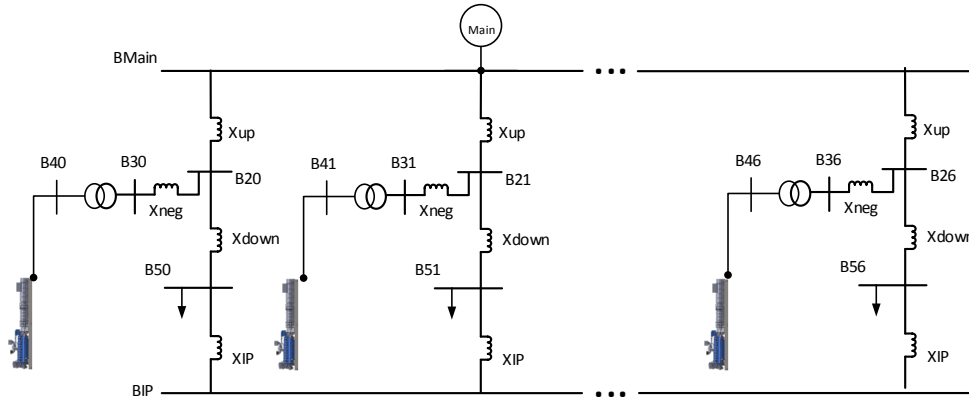


Figure 4.3: IP Start Topology with 7 DRUPS

The test network is shown in Figure 4.3, seven DRUPS are present and one can notice a transformer, with a reactance of 3%, to raise the voltage from 400 V to 11 kV at the terminal of the DRUPS. The active and reactive power drawn by the loads are given in the Table 4.3

Table 4.3: Active and reactive power consumed by the 7 loads

|          | P [kW] | Q [kVar] |
|----------|--------|----------|
| $B_{50}$ | 1000   | 484.32   |
| $B_{51}$ | 800    | 387.46   |
| $B_{52}$ | 600    | 290.59   |
| $B_{53}$ | 1500   | 726.48   |
| $B_{54}$ | 1300   | 629.62   |
| $B_{55}$ | 2000   | 968.64   |
| $B_{56}$ | 1000   | 484.32   |

Table 4.4: Results of the power flow

| | Program | | ARTERE | |
|---|---|---|---|---|
| | $\lvert V \rvert$ | $\theta$ | $\lvert V \rvert$ | $\theta$ |
| $B_{Main}$ | 1 | 0 | 1 | 0 |
| $B_{20}$ | 1.0154882 | -0.1666184 | 1.0154883 | -0.1666184 |
| $B_{30}$ | 0.99723332 | -0.1666184 | 0.99723333 | -0.1666184 |
| $B_{40}$ | 1.0054316 | -0.1666184 | 1.0054317 | -0.1666184 |
| $B_{50}$ | 1 | -0.19979421 | 1 | -0.19979419 |
| $B_{21}$ | 1.0125237 | -0.15505498 | 1.0125238 | -0.15505497 |
| $B_{31}$ | 0.99760291 | -0.15505498 | 0.99760295 | -0.15505497 |
| $B_{41}$ | 1.0043038 | -0.15505498 | 1.0043039 | -0.15505497 |
| $B_{51}$ | 1 | -0.18594677 | 1 | -0.18594676 |
| $B_{22}$ | 1.0096162 | -0.14346989 | 1.0096163 | -0.14346988 |
| $B_{32}$ | 0.9979468 | -0.14346989 | 0.9979469 | -0.14346988 |
| $B_{42}$ | 1.0031876 | -0.14346989 | 1.0031877 | -0.14346988 |
| $B_{52}$ | 1 | -0.17206943 | 1 | -0.17206942 |
| $B_{23}$ | 1.0231467 | -0.19544198 | 1.0231468 | -0.19544196 |
| $B_{33}$ | 0.99619818 | -0.19544198 | 0.99619824 | -0.19544196 |
| $B_{43}$ | 1.0083008 | -0.19544198 | 1.0083009 | -0.19544196 |
| $B_{53}$ | 1 | -0.23429178 | 1 | -0.23429175 |
| $B_{24}$ | 1.0200411 | -0.18392621 | 1.0200412 | -0.18392619 |
| $B_{34}$ | 0.99663119 | -0.18392621 | 0.99663123 | -0.18392619 |
| $B_{44}$ | 1.0071446 | -0.18392621 | 1.0071447 | -0.18392619 |
| $B_{54}$ | 1 | -0.22051257 | 1 | -0.22051254 |
| $B_{25}$ | 1.0311549 | -0.22416233 | 1.0311549 | -0.22416232 |
| $B_{35}$ | 0.99500615 | -0.22416233 | 0.99500612 | -0.22416233 |
| $B_{45}$ | 1.0112406 | -0.22416233 | 1.0112406 | -0.22416233 |
| $B_{55}$ | 1 | -0.26863493 | 1 | -0.26863492 |
| $B_{26}$ | 1.0154882 | -0.16661841 | 1.0154883 | -0.16661840 |
| $B_{36}$ | 0.99723331 | -0.16661841 | 0.99723333 | -0.16661840 |
| $B_{46}$ | 1.0054316 | -0.16661841 | 1.0054317 | -0.16661840 |
| $B_{56}$ | 1 | -0.19979421 | 1 | -0.19979419 |
| $B_{IP}$ | 0.99954673 | -0.21157493 | 0.99954677 | -0.21157491 |

The results of the power flow problem are given in Table 4.4. As it can be seen, the solution given by the program are very closed to the solution provided by ARTERE. The error is in the order of a few millionths of percent, which is negligible. Some observations can be made, as the machines are in conditioning mode, one can notice that the phase angle of buses "$B_2x$", "$B_3x$" and "$B_4x$" are the same which correspond to a null active power flow. An other observation can be point out, the load voltage magnitudes are equal to 1 pu following the application of the sensitivity analysis.

In conclusion, two validations test have been performed, the first one to ensure that the program can get results which are confirmed by an analytic reasoning and the second one to show that the program can find results that are same as a power flow software. This bodes well for the following study cases.

# 3  Case Study

The power flow studies are important. Indeed, EURO-DIESEL can not sell N DRUPS placed in an IP star configuration if these studies show that the system is not N-1 secure or, sometimes, N-2 secure. Thus, depending on the results obtained, one will increase or decrease the number of units, adapt the value of the IP Choke to limit the short circuit current or change the distribution of the loads.

In this particular case, the specifications provided by the customer include a network with 5 DRUPS, in an IP star topology, the number of loads, their active and reactive consumption and the scenarios to perform. The loads active power are given in Table 4.5

<div align="center">

Table 4.5: Active power consumed by the loads in kW

| | Unit 1 | Unit 2 | Unit 3 | Unit 4 | Unit 5 |
|---|---|---|---|---|---|
| Unit 1 | 0 | 650 | 650 | 0 | 0 |
| Unit 2 | 650 | 0 | 650 | 0 | 0 |
| Unit 3 | 650 | 650 | 0 | 0 | 0 |
| Unit 4 | 0 | 0 | 0 | 0 | 1050 |
| Unit 5 | 0 | 0 | 0 | 1050 | 0 |
| Total | 1300 | 1300 | 1300 | 1050 | 1050 |

</div>

The DRUPS have an output power of 2250 kVA which corresponds to a maximum active power output of 1800 kW. So, there is redundancy since the maximum active power produced by the DRUPS is equal to 9000 kW and the total active power drawn by the loads is equal to 6000 kW.

The loads 1, 2 and 3 are IT loads with a power factor of 0.9 lagging and the loads 4 and 5 are mechanical loads with a power factor of 0.85 lagging. The Table 4.6 gives the reactive power drawn by the loads.

<div align="center">

Table 4.6: Reactive power consumed by the loads in kVar

| | Unit 1 | Unit 2 | Unit 3 | Unit 4 | Unit 5 |
|---|---|---|---|---|---|
| Unit 1 | 0 | 314.81 | 314.81 | 0 | 0 |
| Unit 2 | 314.81 | 0 | 314.81 | 0 | 0 |
| Unit 3 | 314.81 | 314.81 | 0 | 0 | 0 |
| Unit 4 | 0 | 0 | 0 | 0 | 650.73 |
| Unit 5 | 0 | 0 | 0 | 650.73 | 0 |
| Total | 629.62 | 629.62 | 629.62 | 650.73 | 650.73 |

</div>

This particular way to specify loads power is explained in Annex A.

As mentioned above, the DRUPS are placed in an IP star topology, as can be seen in Figure 4.4. The case study focus on the conditioning mode. The value of the reactance, given in Table 4.1 are mainly chosen

with respect to the voltage drop due to a short-circuit current. In fact the reactances are chosen by EURO-DIESEL.
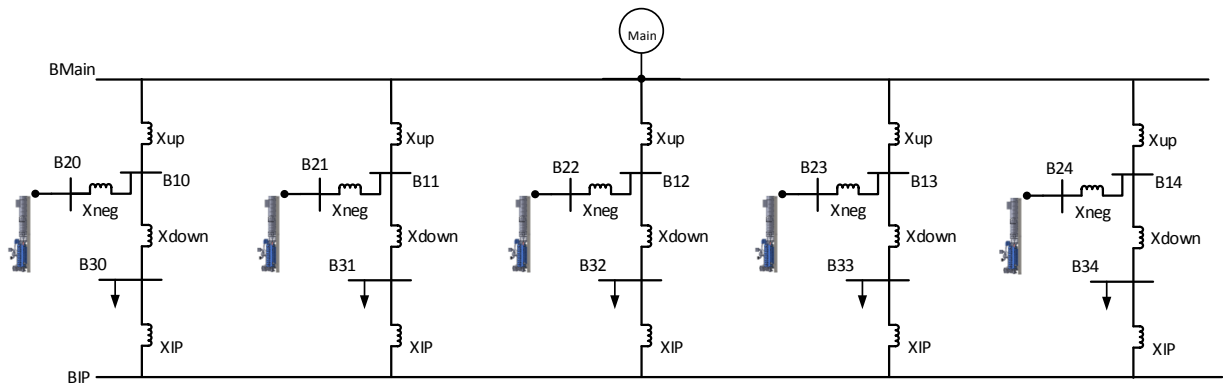


Figure 4.4: IP Star Topology with 5 DRUPS

Table 4.7: Line Impedance

|  | X[pu] |
|---|---|
| $X_{up}$ | 0.3852 |
| $X_{down}$ | 0.0770 |
| $X_{neg}$ | - 0.0642 |
| $X_{IP}$ | 0.292 |

First of all, one must check if the lines are not overloaded in normal operation mode, that is to say, when the 5 units are in operation. An alarm is triggered if the active power flowing through QD2 exceed the maximum active power that a DRUPS can supply. The Table 4.8 displays the important results of the problem studied.

Table 4.8: Important Results for the Normal Stage

|  | Unit 1 | Unit 2 | Unit 3 | Unit 4 | Unit 5 |
|---|---|---|---|---|---|
| Active load [kW] | 1300 | 1300 | 1300 | 1050 | 1050 |
| Reactive load [kVAR] | 629.62 | 629.62 | 629.62 | 650.73 | 650.73 |
| Active Power to IP ring [kW] | -61.27 | -61.27 | -61.27 | 91.91 | 91.91 |
| Reactive Power to IP ring [kVAR] | 0.52 | 0.52 | 0.52 | 0.78 | 0.78 |
| Active Power through QD2 [kW] | 1238.72 | 1238.72 | 1238.72 | 1141.91 | 1141.91 |
| Reactive Power through QD2 [kVAR] | 630.14 | 630.14 | 630.14 | 651.51 | 651.51 |
| Apparent Power through QD2 [kVA] | 1389.79 | 1389.79 | 1389.79 | 1314.70 | 1314.701 |

As can be observed in the Table above, none of the lines are overloaded since the active power is below 1800 kW. In fact, the active power flowing through QD2 are the biggest for Unit 1, 2 and 3 and it is only at 68.8 % of the maximum acceptable power. One can also highlight an active load sharing through the IP choke even in conditioning mode. Intuitively, this result can be anticipated since it is a parallel topology with the same line characteristics but the load distribution is unbalanced. Another observation can be made, the reactive power flowing to the IP ring is nearly null, indeed, the high value of the IP choke opposes the flowing of the reactive power.

For the remainder of this study, three scenarios will be detailed. Firstly, the lost of one DRUPS will be simulated and the IP choke is bypassed, so that the downstream load is placed on the IP bus. Secondly, the loss of distribution switchboard will be simulated, that is to say, one load is re-distributed towards other distribution units and moreover only four units and the mains are supplying the power. And thirdly, the lost of two DRUPS will be simulated.

**First Scenario : Loss of one DRUPS**

This scenario is carried out to ensure the customer that the system is N-1 secure. This operating point must still supply the loads without any problems, in fact, the maintenance of one DRUPS at a time can happen.

Table 4.9: Important Results of the Loss of DRUPS 1

|  | Unit 1 | Unit 2 | Unit 3 | Unit 4 | Unit 5 | IP Bus |
|---|---|---|---|---|---|---|
| Active load [kW] | 0 | 1300 | 1300 | 1050 | 1050 | 1300 |
| Reactive load [kVAR] | 0 | 629.62 | 629.62 | 650.73 | 650.73 | 629.62 |
| Active Power to IP ring [kW] | 0 | 248.81 | 248.81 | 401.18 | 401.18 | |
| Reactive Power to IP ring [kVAR] | 0 | 170.32 | 170.32 | 175.94 | 175.94 | |
| Active Power through QD2 [kW] | 0 | 1548.81 | 1548.81 | 1451.18 | 1451.18 | |
| Reactive Power through QD2 [kVAR] | 0 | 799.94 | 799.94 | 826.67 | 826.67 | |
| Apparent Power through QD2 [kVA] | 0 | 1743.19 | 1743.19 | 1670.13 | 1670.13 | |

In Table 4.9, the loss of Unit 1 is observed. The active power flowing through QD2 increases for the four remaining units which is coherent since the load, which was initially in unit 1, is now connected to the IP bus. It can be observed that the maximum active power flowing through QD2 is not reached, for units 2 and 3, it is at 86 %. A critical point needs also to be highlight, it is the magnitude of the voltage at the IP bus which is only at 0.9814 pu. This latter is somewhat low for the critical load but in this topology, the reactive load sharing is disabled which means that the DRUPS only regulate their downstream load and not the load on the IP bus.

The other cases, where the units 2 and 3 are lost, are not developed since it will reproduce the same results as Table 4.9. The loss of units 4 and 5 will produce the same results, so the power flow solution for the loss of unit 4 will only be consider.

Table 4.10: Important Results of the Loss of DRUPS 4

|  | Unit 1 | Unit 2 | Unit 3 | Unit 4 | Unit 5 | IP Bus |
|---|---|---|---|---|---|---|
| Active load [kW] | 1300 | 1300 | 1300 | 0 | 1050 | 1050 |
| Reactive load [kVAR] | 629.6 | 629.62 | 629.62 | 0 | 650.73 | 650.73 |
| Active Power to IP ring [kW] | 224.42 | 224.42 | 224.42 | 0 | 376.72 | |
| Reactive Power to IP ring [kVAR] | 172.91 | 172.91 | 172.91 | 0 | 178.10 | |
| Active Power through QD2 [kW] | 1524.42 | 1524.42 | 1524.42 | 0 | 1426.72 | |
| Reactive Power through QD2 [kVAR] | 802.53 | 802.53 | 802.53 | 0 | 828.83 | |
| Apparent Power through QD2 [kVA] | 1722.76 | 1722.76 | 1722.76 | 0 | 1649.99 | |

The results of the loss of unit 4 are shown in Table 4.10. As can be noticed, the power flowing through the lines are smaller than the results of the loss of unit 1. Actually, this is normal because the load transfers to the IP bus is smaller and , for this case, the power flowing through QD2 for units 1, 2 and 3 is at 84.69% of the maximum allowed. One last observation can be made, this is the IP bus voltage, it is at 0.9811 pu which is somewhat lower than the previous case because the reactive load is higher.

Despite the fact that the network approaches the critical operating point, one can states that the network is indeed N-1 secure.

**Second Scenario : Loss of one distribution switchboard**

For this case, the operating point should be closer to the limit, especially for the active power flowing through QD2. In fact, the loss of a distribution switchboard means that the load is re-distributed towards other distribution units and there is, additionally, a trip of a DRUPS. The load is no more placed on the IP bus, which means that the 4 units are no longer supplying together the load.

Table 4.11: Important Results of the Loss of Distribution Switchboard 1

|  | Unit 1 | Unit 2 | Unit 3 | Unit 4 | Unit 5 |
|---|---|---|---|---|---|
| Active load [kW] | 0 | 1950 | 1950 | 1050 | 1050 |
| Reactive load [kVAR] | 0 | 944.43 | 944.43 | 650.73 | 650.73 |
| Active Power to IP ring [kW] | 0 | -271.2 | -271.2 | 271.2 | 271.2 |
| Reactive Power to IP ring [kVAR] | 0 | 8.19 | 8.19 | 8.19 | 8.19 |
| Active Power through QD2 [kW] | 0 | 1678.8 | 1678.8 | 1321.2 | 1321.2 |
| Reactive Power through QD2 [kVAR] | 0 | 952.62 | 952.62 | 658.92 | 658.92 |
| Apparent Power through QD2 [kVA] | 0 | 1930.24 | 1930.24 | 1476.39 | 1476.39 |

The first distribution switchboard that we lose is at the unit 1 as can be seen in Table 4.11. The active power flowing through QD2 for units 2 and 3 is indeed higher than the case shown in Table 4.9. The latter is at 93.3 % of the maximum active power, so one can noticed that the limit is almost reached. There is also an active load sharing as happening in normal operation but no reactive load sharing.

As mentioned before, the loss of the second or third distribution switchboard brings no additional information. So for the next loss, one directly trips the fourth distribution switchboard.

Table 4.12: Important Results of the Loss of Distribution Switchboard 4

|  | Unit 1 | Unit 2 | Unit 3 | Unit 4 | Unit 5 |
|---|---|---|---|---|---|
| Active load [kW] | 1300 | 1300 | 1300 | 0 | 2100 |
| Reactive load [kVAR] | 629.6 | 629.62 | 629.62 | 0 | 1301.46 |
| Active Power to IP ring [kW] | 117.44 | 117.44 | 117.44 | 0 | -352.33 |
| Reactive Power to IP ring [kVAR] | 3.07 | 3.07 | 3.07 | 0 | 9.21 |
| Active Power through QD2 [kW] | 1417.44 | 1417.44 | 1417.44 | 0 | 1747.66 |
| Reactive Power through QD2 [kVAR] | 632.69 | 632.69 | 632.69 | 0 | 1310.67 |
| Apparent Power through QD2 [kVA] | 1552.23 | 1552.23 | 1552.23 | 0 | 2184.53 |

One can compare the results in Table 4.11 to the results in Table 4.12 and discern that the lines for unit 2 and 3 are less loaded but with counterpart the power flowing through QD2 for unit 5 reached 97.1 % of the acceptable limit.

Nevertheless, the redundancy of the system allows a loss of any distribution switchboard.

**Third Scenario : Loss of two DRUPS**

For this scenario, two DRUPS are tripped at the same time to see if the system is N-2 secure. In fact, this scenario overloads the three remaining DRUPS which means that during the transient period, see Chapter 1, the DRUPS will automatically trip in return. In Table 4.13, One can see that the active power flowing through QD2 for the remaining units is in excess, especially for the unit 3 where the active power is 15 % above the maximum power allowed.

Table 4.13: Important Results of the Loss of DRUPS 1 and 2

|  | Unit 1 | Unit 2 | Unit 3 | Unit 4 | Unit 5 | IP Bus |
|---|---|---|---|---|---|---|
| Active load [kW] | 0 | 0 | 1300 | 1050 | 1050 | 2600 |
| Reactive load [kVAR] | 0 | 0 | 629.62 | 650.73 | 650.73 | 1259.23 |
| Active Power to IP ring [kW] | 0 | 0 | 766.25 | 916.87 | 916.87 | |
| Reactive Power to IP ring [kVAR] | 0 | 0 | 525.80 | 540.79 | 540.79 | |
| Active Power through QD2 [kW] | 0 | 0 | 2066.25 | 1966.87 | 1966.87 | |
| Reactive Power through QD2 [kVAR] | 0 | 0 | 1155.42 | 1191.52 | 826.67 | |
| Apparent Power through QD2 [kVA] | 0 | 0 | 2367.36 | 2299.63 | 2299.63 | |

In conclusion, for the latter scenario, we notice that the system is not N-2 secure.

Before completing the study for the customer, it is necessary to study the effects of the three phases short-

circuit.

**Three Phases Short-Circuit**

The three phases faults are the most severe fault under which the dimensioning of the lines and the calibration of the breakers are chosen. For that, a fictitious zero impedance fault will be simulated on IP bus and on a load. The topology selected is the one with the reactance of the IP choke equals to 29.2 %.

The first case studied is the simulation of a short-circuit on IP bus.

Table 4.14: Voltage profile before and after the fault

| | Before Fault | | After Fault | |
| --- | --- | --- | --- | --- |
| | $|V|$ | $\theta$ | $|V|$ | $\theta$ |
| $B_{Main}$ | 1 | 0 | 1 | 0 |
| $B_{10}$ | 1.0225 | -0.2089 | 0.9492 | -0.2029 |
| $B_{20}$ | 0.9957 | -0.2089 | 0.778 | -0.1871 |
| $B_{30}$ | 1 | -0.2504 | 0.7380 | -0.2375 |
| $B_{11}$ | 1.0225 | -0.2089 | 0.9492 | -0.2029 |
| $B_{21}$ | 0.9957 | -0.2089 | 0.778 | -0.1871 |
| $B_{31}$ | 1 | -0.2504 | 0.7380 | -0.2375 |
| $B_{12}$ | 1.0225 | -0.2089 | 0.9492 | -0.2029 |
| $B_{22}$ | 0.9957 | -0.2089 | 0.778 | -0.1871 |
| $B_{32}$ | 1 | -0.2504 | 0.7380 | -0.2375 |
| $B_{13}$ | 1.0231 | -0.1923 | 0.9499 | -0.1857 |
| $B_{23}$ | 0.9963 | -0.1923 | 0.7789 | -0.1682 |
| $B_{33}$ | 1 | -0.2305 | 0.7383 | -0.2136 |
| $B_{14}$ | 1.0231 | -0.1923 | 0.9499 | -0.1857 |
| $B_{24}$ | 0.9963 | -0.1923 | 0.7789 | -0.1682 |
| $B_{34}$ | 1 | -0.2305 | 0.7383 | -0.2136 |
| $B_{IP}$ | 1 | -0.2425 | 0 | 0 |

The voltages of the bus, before and after the fault, are shown in Table 4.14. As can be seen, before the fault, the voltages profile are quite decent, as expected the magnitudes of the load voltage are equal to 1 pu and the phase shift between the DRUPS buses and the middle buses are null.

Once the fault appeared, the voltage magnitudes drop which is predicted phenomenon since the current passing through the lines is greater because of the "solid" fault on the IP bus. Even if this incident appeared, the IP choke limits correctly the voltage drop which is equals to almost 26 % but using an IP choke of 41.8 %, the voltage drop is reduced to 20%.

Another event can be observe which is the flow of the active power through the line between the middle buses and the DRUPS buses. In fact, this event can also be anticipated, the speed of the DRUPS will decrease during the first moment of the short-circuit, thus, the mains will supply the active power to the

DRUPS.

However, the interest of this study is to compute the magnitudes of the current produced by the DRUPS which are mainly reactive. These latter are displayed in Table 4.15.

Table 4.15: Magnitude of the current produced by the DRUPS

|  | DRUPS 1 | DRUPS 2 | DRUPS 3 | DRUPS 4 | DRUPS 5 |
|---|---|---|---|---|---|
| I [A] | 275.05 | 275.05 | 275.05 | 275.3 | 275.3 |

One can observe that the magnitudes of the current produced by DRUPS 1, 2 and 3 are different than the DRUPS 4 and 5. It comes from the fact that the load of their unit is different. And finally, the equipment must withstand a current of 1375.8 A, the sum of the currents shown in Table 4.15.

The second case studied is the simulation of a short-circuit on the first load.

Table 4.16: Voltage profile before and after fault

|  | Before Fault | | After Fault | |
|---|---|---|---|---|
|  | $|V|$ | $\theta$ | $|V|$ | $\theta$ |
| $B_{Main}$ | 1 | 0 | 1 | 0 |
| $B_{10}$ | 1.0225 | -0.2089 | 0.7426 | -0.1933 |
| $B_{20}$ | 0.9957 | -0.2089 | 0.1667 | 0 |
| $B_{30}$ | 1 | -0.2504 | 0 | 0 |
| $B_{11}$ | 1.0225 | -0.2089 | 1.004 | -0.2071 |
| $B_{21}$ | 0.9957 | -0.2089 | 0.9406 | -0.2033 |
| $B_{31}$ | 1 | -0.2504 | 0.9338 | -0.2465 |
| $B_{12}$ | 1.0225 | -0.2089 | 1.004 | -0.2071 |
| $B_{22}$ | 0.9957 | -0.2089 | 0.9406 | -0.2033 |
| $B_{32}$ | 1 | -0.2504 | 0.9338 | -0.2465 |
| $B_{13}$ | 1.0231 | -0.1923 | 1.0046 | -0.1904 |
| $B_{23}$ | 0.9963 | -0.1923 | 0.9414 | -0.1862 |
| $B_{33}$ | 1 | -0.2305 | 0.9338 | -0.2258 |
| $B_{14}$ | 1.0231 | -0.1923 | 1.0046 | -0.1904 |
| $B_{24}$ | 0.9963 | -0.1923 | 0.9414 | -0.1862 |
| $B_{34}$ | 1 | -0.2305 | 0.9338 | -0.2258 |
| $B_{IP}$ | 1 | -0.2425 | 0.747 | -0.2362 |

As one may notice, the profile of the voltages from Table 4.16, after the fault, is relatively different from Table 4.14. The voltages for the units 2, 3, 4 and 5 are almost kept at their post fault voltages, indeed, these buses are electrically far from the fault. More precisely, one can observe that the voltage drop for the renaming load buses is approximately 7% and 5% if the IP choke of 41.8 % is placed. Whereas the voltages of unit 1 drastically drop, especially for the DRUPS bus which is now equal to 0.1667 pu.

Some observations are the same, as the three phases fault on the IP bus, such as the flow of active power toward the DRUPS. By looking at the phase shift between buses $B_{10}$ and $B_{20}$, one can deduce that there is some active power flowing through this line but the phase shift between buses $B_{1x}$ and $B_{2x}$ $\forall$ x $\in$ 1,...,4 are minimal. The physical interpretation of those phenomenons is that the DRUPS near the fault slows sharply and the others feel less the effect of the short-circuit.

The conclusion of these two simulations is that the choice of the IP choke is a crucial point for the isolation of the units and the limitation of short-circuit effects. Indeed, by placing high reactance values, one can limit the short-circuit current and at the same time the voltage drop.

The last part focuses on the limit that the IP choke value can take in the case currently investigated.

**Limitation**

The isolation between the different units is fundamental in case of a short-circuit on the IP bus. In fact, the greater the value of the IP choke the better it is to limit the voltage drop on the load in case of a short-circuit and the short-circuit current.

As explained in Chapter 2, the IP choke should be kept as low as possible to limit the voltage drop in case of a loss of unit. The Figure 4.5 shows the evolution of the voltage drop for the fourth load with respect to the value of the IP choke at the moment when QDR is still open which means that the IP choke is not bypass yet. One can observe that the voltage drop nearly grows exponentially and when passed the value of 47.5 % for the choke, the program do not converge any more. Indeed, the maximum power transmitted to a load is reached which can be notice by looking at the PV curve for a power factor of 0.85.
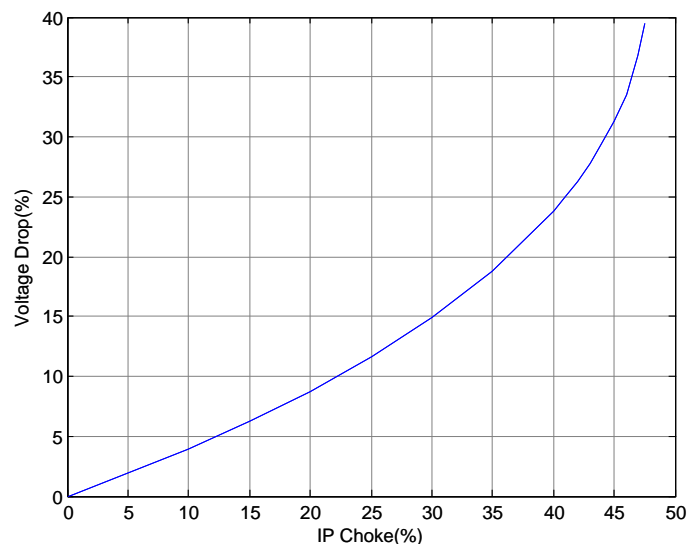


Figure 4.5: Evolution of Voltage Drop with respect to the IP Choke

Another physical constraint can be observe if one increases the value of the choke until 41.8%. The units become more and more isolated, in consequence the active power shared through the IP bus is less pro-

nounced. So, for example, when there is a loss of the fourth distribution switchboard, the active power flowing through QD2 can reach the maximum active power that one DRUPS can provide. If one keep increasing the IP choke value, the DRUPS will not be able to supply the load during the transient period.

The Table 4.17 highlights this specific case. The active power flowing through QD2 for the fourth unit indeed reaches 1800 kW.

Table 4.17: Important Results of the Loss of Distribution Switchboard 4

|  | Unit 1 | Unit 2 | Unit 3 | Unit 4 | Unit 5 |
|---|---|---|---|---|---|
| Active load [kW] | 1300 | 1300 | 1300 | 0 | 2100 |
| Reactive load [kVAR] | 629.6 | 629.62 | 629.62 | 0 | 1301.46 |
| Active Power to IP ring [kW] | 99.95 | 99.95 | 99.95 | 0 | -299.87 |
| Reactive Power to IP ring [kVAR] | 3.71 | 3.71 | 3.71 | 0 | 11.15 |
| Active Power through QD2 [kW] | 1399.95 | 1399.95 | 1399.95 | 0 | 1800.12 |
| Reactive Power through QD2 [kVAR] | 633.33 | 633.33 | 633.33 | 0 | 1312.61 |
| Apparent Power through QD2 [kVA] | 1536.55 | 1536.55 | 1536.55 | 0 | 2227.87 |

It must be highlight that the choice of the IP choke value should be a trade off between the limitation of the short-circuit current and the effects observed above.

This completes the static modeling and now we will focus on the dynamic modeling in the following chapters.

# Part III

# Dynamic Modeling

# Purpose of This Part

The numerical simulation of the dynamic response of a NO-BREAK KS® has, so far, never been investigated by EURO-DIESEL. So this part of the thesis will be devoted to this important study.

To reach this goal, this dynamic modeling part will be divided into three Chapter. The first chapter will introduce the software RAMSES as well as the user interaction to create and add a new model in RAMSES. Then the second chapter will describe the models developed for the excitation and torque controls of the NO-BREAK KS®. And finally, for the third section, the models will be used in RAMSES to simulate the response of the NO-BREAK KS®.

# Chapter 5

# Interaction with RAMSES [9]

The powerful software RAMSES, developed by Pr Thierry Van Cutsem, is used in order to simulate the dynamic response of the DRUPS. In fact, the acronym RAMSES stands for RApid Multiprocessor Simulation of Electric power Systems. As can be seen in Figure 5.1, this software includes three main parts : the power system modeling, the software implementation and the acceleration techniques [10].
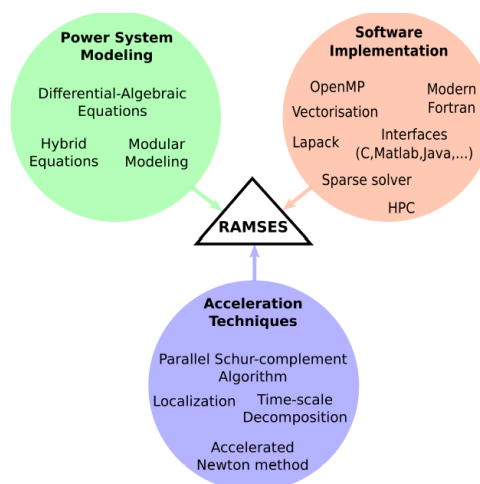


Figure 5.1: RAMSES Components

For this master thesis, we will add two power system models and work with modern Fortran codes. Indeed, the models of excitation and torque controls of a DRUPS are not implemented in RAMSES. Subsequently, we will describe the way to introduce models in RAMSES by means of CODEGEN utility.

As can be seen in Figure 5.2, there are two different ways to add a model on RAMSES. A way that can be called "direct" where one can directly code the model in Fortran which will be compile with the rest of RAMSES [K]. And another way is to implement models in RAMSES with the CODEGEN utility.
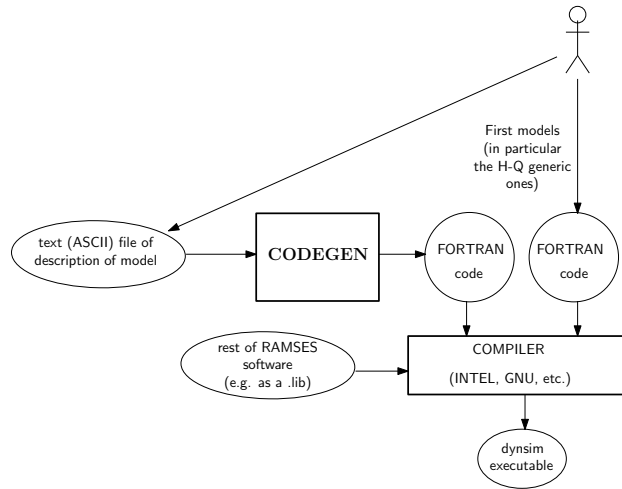
Figure 5.2: User Interaction

The CODEGEN utility takes as input a text (ASCII) file which describes the model and gives as output a Fortran code which will be compile with the rest of RAMSES. In fact, four types of model can be implemented : excitation control of synchronous machine model, torque control of synchronous machine model, injector model and two-port model. These latter must be described as it is shown in Figure 5.3.
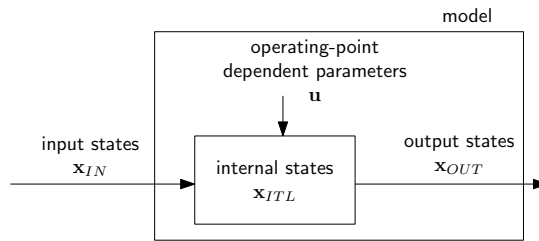


Figure 5.3: Model Description

As mentioned previously, the main purpose is to develop the excitation and torque control of a DRUPS.

The excitation controller can take many input states as : the terminal voltage $V$, the active power produced $P$, the reactive power produced Q, the rotor speed $\omega$ and/or the field current $i_f$. And it gives as output state the field voltage $v_f$. In this application, the only input state is the terminal voltage $V$.

Concerning the torque controller, it can take two input states : the rotor speed $\omega$ and/or active power produced $P$. And it gives as output state the mechanical torque applied to rotor $T_m$. In this study, these two inputs will be introduced.

The complete model is obtained by assembling the models of elementary blocks (e.g. time constants, integrators, PID controllers, etc.) as can be seen in Figure 5.4. Each block contributes with its algebraic and/or differential equations, involving discrete variables **z** if needed. Between the blocks, there are links at which a state of the type $x_{ITL}$ is associated. The user have to give to each of these states a unique name and an
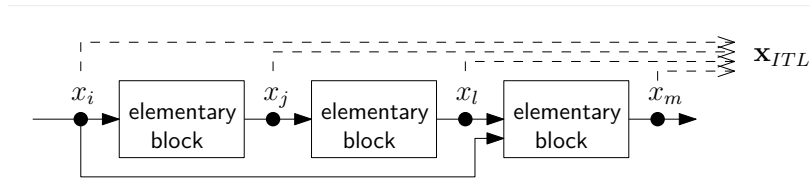
initial value.



Figure 5.4: Model Structure

Finally, the text file must gather all the information concerning a particular model in structured way shown in Figure 5.5.

```
exc                     (type of model : excitation control)
ST6B_PSS3B_lim          (final name of model will be exc_ST6B_PSS3B_lim)

%data                   (names data to be read on data file)
...
%parameters             (operating-point dependent parameters u)
...
%states                 (states associated to links between elementary blocks
...
%observables            (states available for display at end of simulation)
...
%models                 (list of elementary blocks)
...
```

Figure 5.5: File Structure

The way to implement a model in RAMSES has been developed. So, we can now derive the models.

# Chapter 6

# Derivation of the Models

In order to have a dynamic study for the response of the NO-BREAK KS®, the exciter and the speed governor must be detailed as explained in Chapter 5. At first, the exciter model will be established and then the diesel governor model.

Some values which are in the following models will be kept hidden since it belongs to the industrial secret.

## 1 Exciter Model

The DRUPS manufactured by EURO-DIESEL uses a field-controlled alternator-rectifier excitation systems with system-supplied electronic voltage regulators [11]. The output voltage of the regulator is a function of the terminal voltage. In that case, the use of a PI controller is suitable to quickly damped an overshoot and correct the steady-state error. More precisely, the real controller implemented is a PS(proportional-summation) controller since it is a discrete time system implemented in a PIC microcontroller. However, RAMSES works in a way that it needs continuous time system to simulate the behavior of a DRUPS.

The excitation system is working during both mode, conditioning and independent. The model used for the simulations is shown in Figure 6.1 .
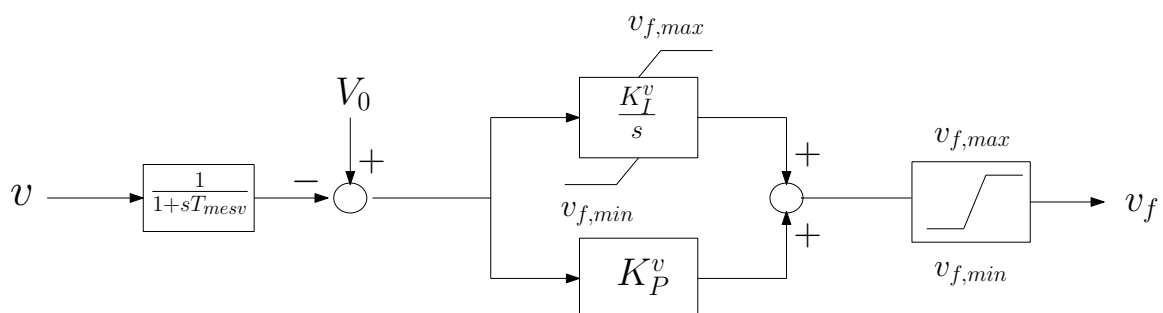


Figure 6.1: Bloc diagram of the exciter model

One can notice that the terminal voltage of the DRUPS, $v$, is first delayed by a time constant $T_{mesv}$, indeed, in reality, the measurements are not instantaneous. The measure voltage is then compare to a voltage setpoint $V_0$, if the error is different from 0, then the PI part of the model act and tries to bring the voltage back to its setpoint value by tuning the field voltage $v_f$. One can also observe a non windup integrator to prevent the integral terms to accumulate a significant error during the rise and thus decrease the overshoot. The last part of the exciter model is a limiter which bounds the value of $v_f$ so it never exceeds the physical, maximum and minimum, values of $v_f$.

# 2    Diesel Governor Model

The diesel governor is either a speed control or a torque control for the DRUPS produced by EURO-DIESEL but in the following simulations, only the torque controller is developed. In fact, it depends on the diesel engine manufacturer and for this master thesis, one will work with a particular manufacturer which requires a torque controller. The Diesel Governor Model, developed in this master thesis, is only used for the independent mode.

The bloc diagram of the torque controller can be seen in Figure 6.2. One can observe two main parts in the bloc diagram, the upper part is the PI controller to bring back the speed of the DRUPS to 1 pu and the lower part is the PI controller which takes care of the active load sharing. As for the terminal voltage in Figure 6.1, the speed $w$ and the active power produced by the DRUPS $P$ are delayed by time constant, respectively, $T_{mesw}$ and $T_{mesp}$. The interesting part is that all the DRUPS of a network share the same setpoint for the speed and the active power. More precisely, for the latter, it is the mean of active power produced by all DRUPS. There is, then, the PI parts of the controller with the non windup integrator and the limiter of the torque values. At last, one can see an additional transfer function with a time constant $T_{delay}$ which is an image of the delay between the moment when the new torque value is computed and the moment when the mechanical torque of the diesel engine is really set to this value.
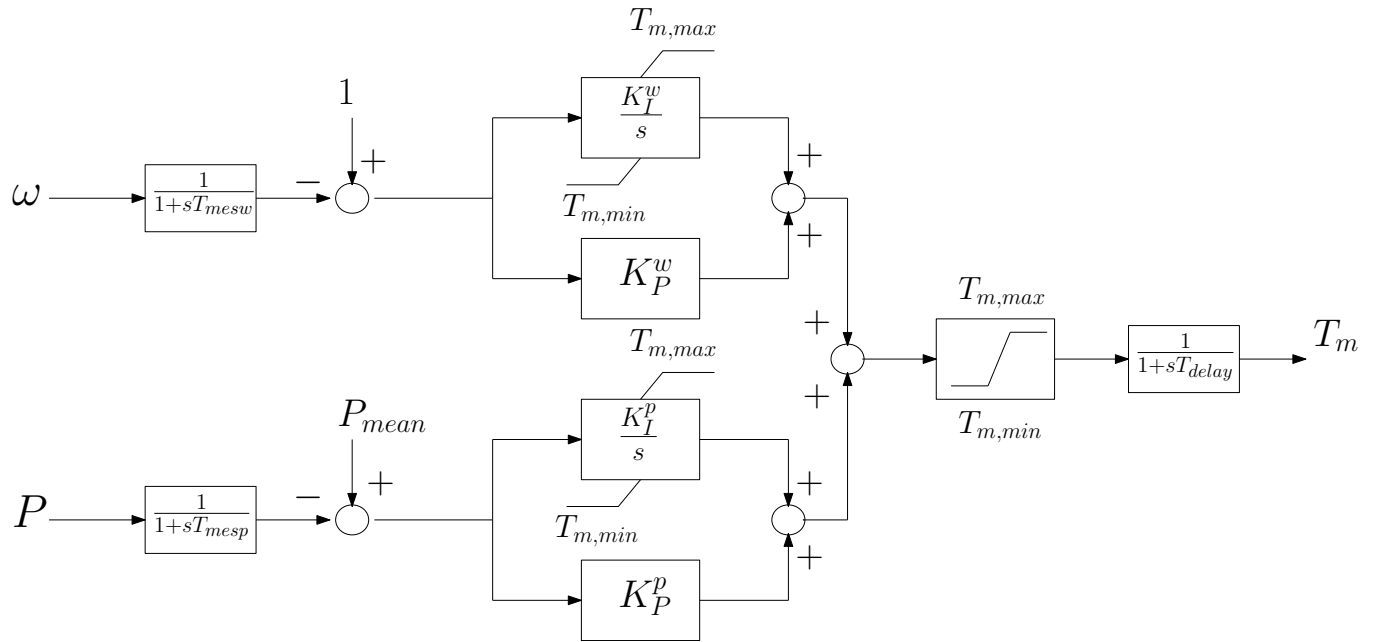
Figure 6.2: Bloc diagram of Torque controller

Concerning the load sharing part, the implementation of a discrete controller was needed to, at the end of each time step, update the value $P_{mean}$ for every torque controller.

The excitation and torque controller have been detailed for CODEGEN utility. The purpose of the following is to find by try-and-error the PI-controller constants of theses models.

# Chapter 7

# Results using the Models

There will be two main parts in this section. On the one hand, we will compare the numerical responses to real factory responses of the DRUPS. And on the other hand, tests with different scenarios will be carried on in order to check the stability limits of the NO-BREAK KS® in the IP star topology.

## 1  Validation Test of The Models

The two models needed for the simulations have been developed before in Chapter 6. Since it was hard to have access to the values of the PI controller, a try-and-error approach was used to find the proportional and integral constants. The simulations results are compared to the real behavior of a DRUPS after steps of load. The DRUPS used for the simulations is a NO-BREAK KS7® (S=2.625 MVA) , one of the most powerful machine produced by EURO-DIESEL. The data for the simulations are display in Table 7.1. The latter are given in per unit in the basis of the alternator.

Table 7.1: Data of the NO-BREAK KS7®

|  | Value [pu] |
|---|---|
| $X_d$ | 2.26 |
| $X_d'$ | 0.268 |
| $X_d''$ | 0.122 |
| $X_q$ | 1.27 |
| $X_q''$ | 0.125 |
| $X_l$ | 0.085 |
| $R_a$ | 0.004 |
| $T_{d0}'$ | 5.048 |
| $T_{d0}''$ | 0.032 |
| $T_{q0}''$ | 0.12 |

The synchronous machine model implemented in RAMSES needs additional information such that the open-

circuit magnetic characteristic and more precisely the saturation factors m and n in eq. (7.1). The curve shown in Figure 7.1 represents the terminal voltage versus the field current of the DRUPS studied. The blue curve tries to fit as well as possible the sample took from the real no-load characteristic curve. But the alternator of EURO-DIESEL has a residual magnetic field since when the field voltage in null the terminal voltage is not 0. RAMSES is implemented in a way that when the terminal voltage is 0, the field voltage must be 0.

The blue curve is found by using non-linear least squares technique to fit a suitable function. The fitted equation of the curve is the following [12],

$$I_{fd} = E_Q(1 + m(E_Q)^n) \tag{7.1}$$

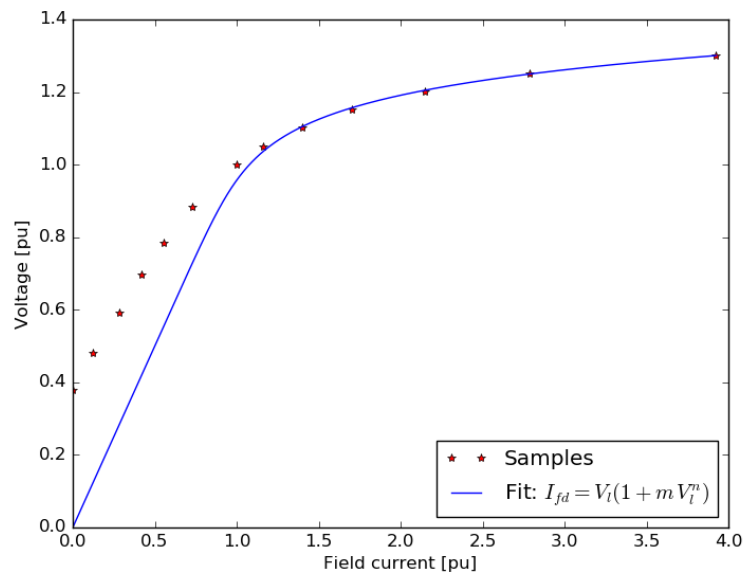And we find n = 12.387 and m = 0.0777.



Figure 7.1: Saturation curve

The synchronous machine model also needs the inertia constant value. The latter is the ration between the stored energy at rated speed and the power of the machine [13]. The equation of the inertia constant is

$$H = 5.48\text{x}10^{-9}\frac{J(RPM)^2}{S} \tag{7.2}$$

In conditioning mode, H = 2.5 and in independent mode, H = 3. The difference comes from coupling with the diesel engine in independent mode.

The first simulation, in conditioning mode, carried on is to find the $K_p^v$ and $K_I^v$ constants for the latter stability tests. In this particular case, a load variation is done in the factory to test the response of one DRUPS as can be seen in Figure 7.2.
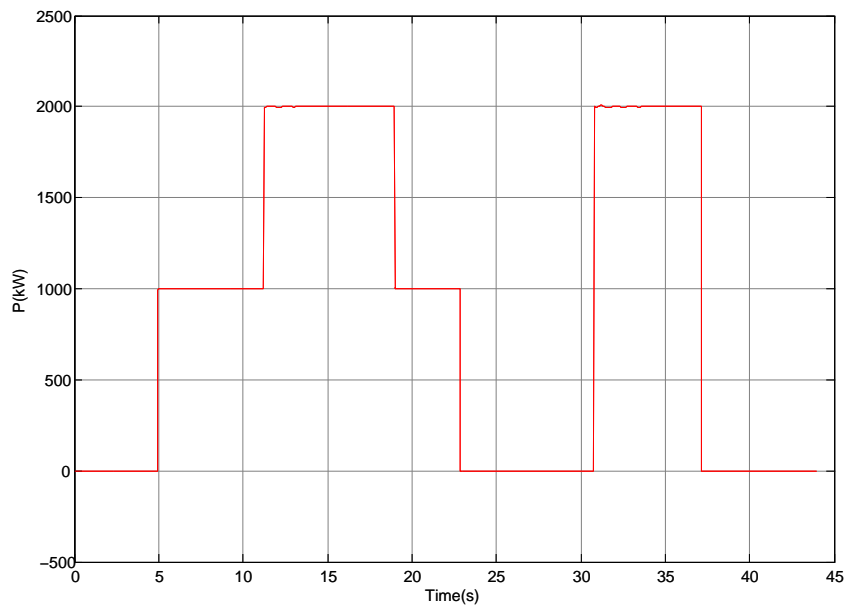


Figure 7.2: Load variation in conditioning mode

In Figure 7.3, one can observe a blue curve which illustrates the variation of the terminal bus voltage during the factory acceptance test to this particular scenario and a red curve which illustrates the response of the DRUPS with RAMSES. Overall, those two curves have the same response apart from the damping of oscillations, indeed, the theoretical oscillations are damped quickly compared to the real oscillations.
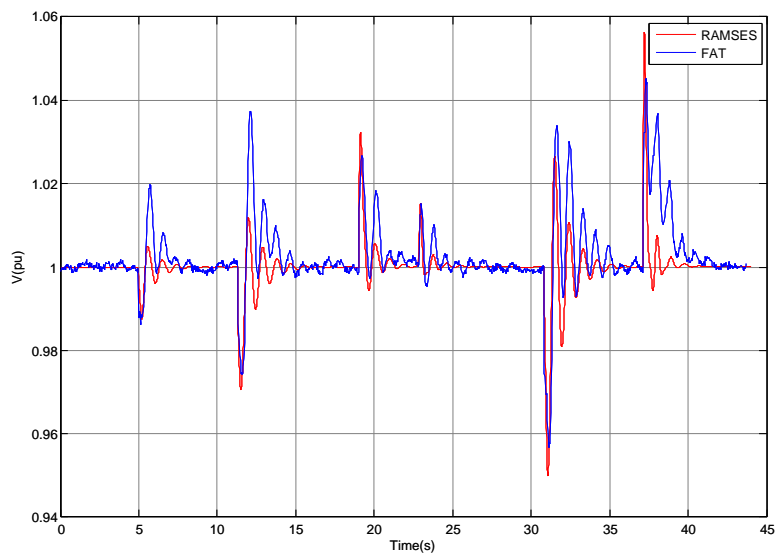


Figure 7.3: Voltage Magnitude of the Load Computed with RAMSES versus the Real Voltage Magnitude

The second simulation, in independent mode, is made to find the values of $K_p^w$ and $K_I^w$. The calibration of these latter is based on a real curve from a factory acceptance test (FAT) which is represented in blue in Figure 7.4. The test is an instantaneous connection of a 1 MW load. The speed of the DRUPS drops as expected and recover after about 3.5 seconds. The curve extracted form RAMSES, the red one, follows closely the response of the DRUPS but one can observe some differences due to the simplicity of the governor model, indeed the dynamic of the time response of the diesel motor is only represented by a time constant $T_{delay}$.
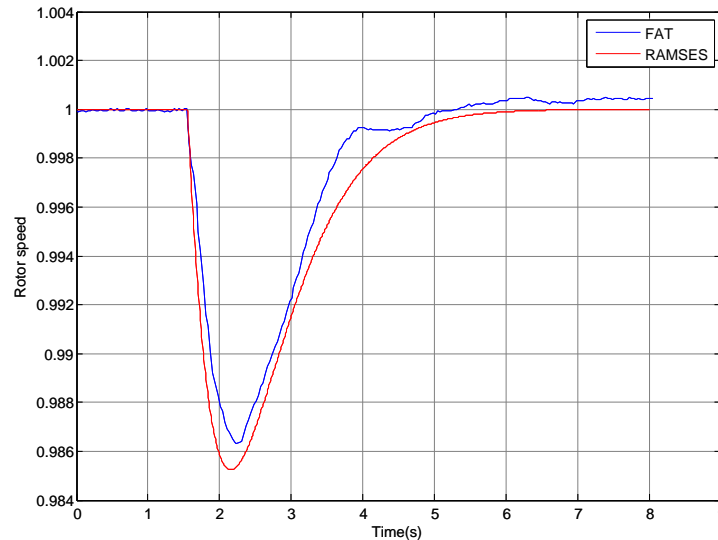


Figure 7.4: Comparison of the Rotor Speed between the Simulation and the Real Response

The try-and-error tests has been carried on to find the PI controller constants that match as well as possible the real time response of the NO-BREAK KS®. In the following section, the complete models will be used to demonstrate that instability, due mainly to the topology, can occur.

## 2 Stability Test

The goal of this section is to highlight the stability limits of the IP topology when the DRUPS are supplying the loads by means of two scenarios. The first scenario will shown the response of two DRUPS, as a result of a load variation, in an IP star topology where the IP choke value is high. The second scenario will focus on the response of three DRUPS following a load variation and in the same topology but now the IP choke reactance will be a conventional one.

### 2.1 Load Variation Using Big IP Choke Reactance

The topology studied is shown in Figure 7.5, one can see two DRUPS in independent mode and initially, no load is connected to bus B20 nor B21. The reactance chosen are displayed in Table 7.2. The main characteristic of this network is the high value of the IP choke which is said to be unconventional.

69

Table 7.2: Line Data of the Topology

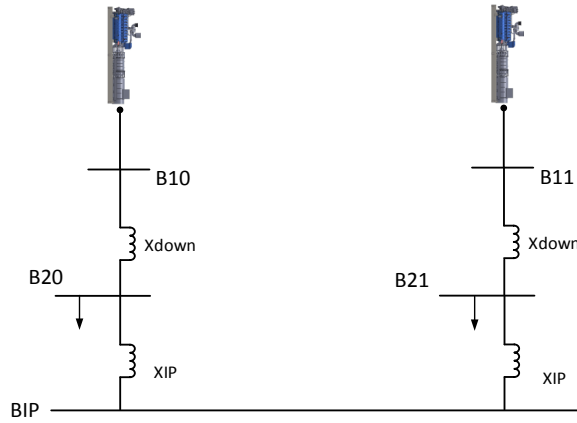| | Value [pu] |
|---|---|
| $X_{down}$ | 0.0134 |
| $X'_{IP}$ | 2.625 |



Figure 7.5: IP Star Topology with 2 Loads

For the following test, one, suddenly, connects a 1 MW load on bus B21 at 5 seconds. The rotor speeds of the two DRUPS are shown in Figure 7.6. During the first moments, following the perturbations, the speed governor of the machines acts very well and bring back the speeds of the machines to 1 pu. Although, at about 24 seconds, the DRUPS are losing their synchronism and the small disturbance rotor angle instability begins.
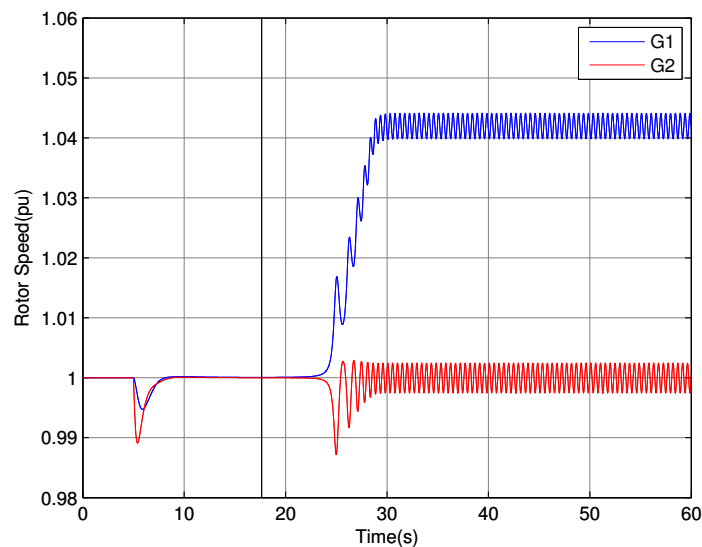


Figure 7.6: Evolution of the Rotor Speed with respect to time

Intuitively, the only reason that can explain this loss of synchronism is the load sharing that happens between the DRUPS. Indeed, as can be seen in Figure 7.7, at 24 seconds, the active power produced by the DRUPS goes in opposite direction and starts oscillating. In fact this can be explained analytically. The following development explains the analytic reason of this loss of synchronism.

The active power flowing through a reactance line is

$$P_{12} = \frac{|V_1||V_2|sin(\theta_1 - \theta_2)}{X} \tag{7.3}$$

So the maximum active power that can flow through this line is when the sine is equal to 1, in other word $\theta_1 - \theta_2 = 90°$, and $|V_1|$ and $|V_2|$ equals to 1.

$$P_{12}^{max} = \frac{1}{X} \tag{7.4}$$

In this case, one can see that the maximum active that can flow from bus B20 to B21 is

$$P_{12}^{max} = \frac{1}{2 * 2.625} = 0.1905 \; pu \tag{7.5}$$

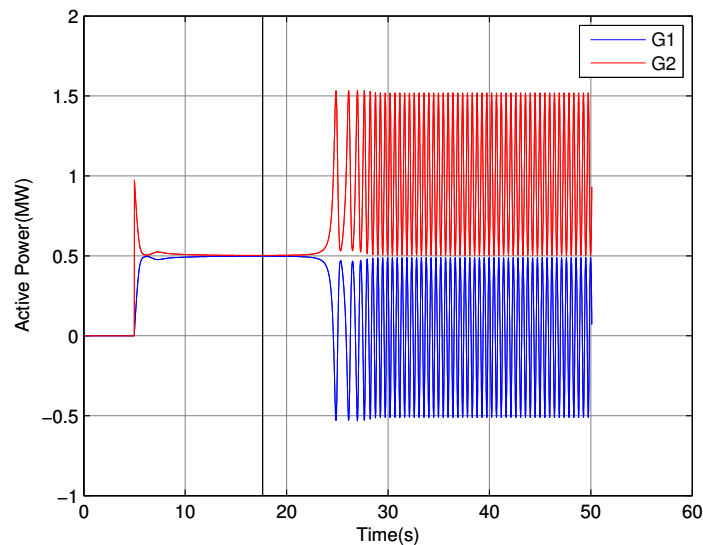Or in MW, $P_{12}^{max} = 0.5$ MW.



Figure 7.7: Evolution of the Active Power produced by The DRUPS

The analytical explanation is based on a hypothesis which states that $\theta_1 - \theta_2 = 90°$. In Figure 7.8, One can observe that the difference of voltage phase angle is 90°at exactly 17.632 seconds which is highlight by a black vertical line. Thus the instability happens at this mark.
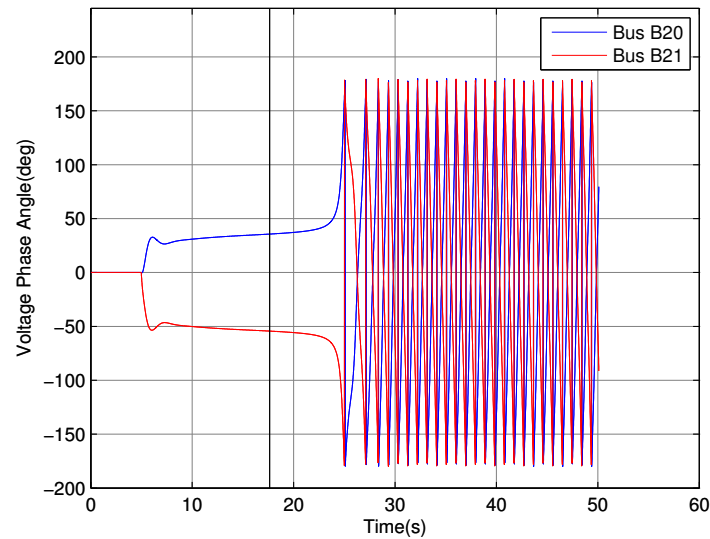


Figure 7.8: Evolution of the Voltage Phase Angle

A first transient instability has been shown by using high reactance value for the IP choke. Let now use a conventional reactance value for the IP choke to find the stability limit of the system.

## 2.2    Load Variation Using Conventional IP Choke Reactance

For the stability test, the topology of the network is shown in Figure 7.9. This time, there are three DRUPS and three loads and the data of the lines are shown in Table 7.3. The IP choke placed is a 30% reactance which is conventionally used by EURO-DIESEL.

Table 7.3: Line Data of the Topology

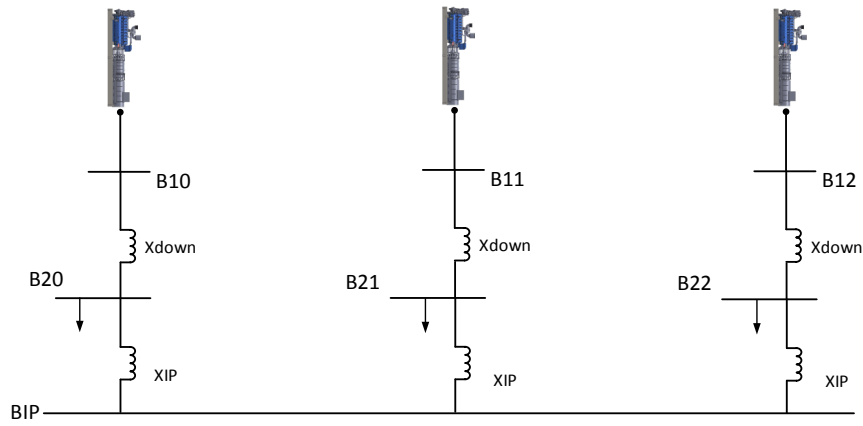|            | Value [pu] |
| ---------- | ---------- |
| $X_{down}$ | 0.0134     |
| $X_{IP}$   | 0.3        |

Figure 7.9: IP Star Topology with 3 Loads

Initially, the three loads does not consumed any power and at the 5 seconds mark, one connects a load on bus B21 of 5 MW. The rotor speed deviation can be observed in Figure 7.10, the latter decreases from about 2.5 % which proves that it is a significant disturbance. However the system recovers well.
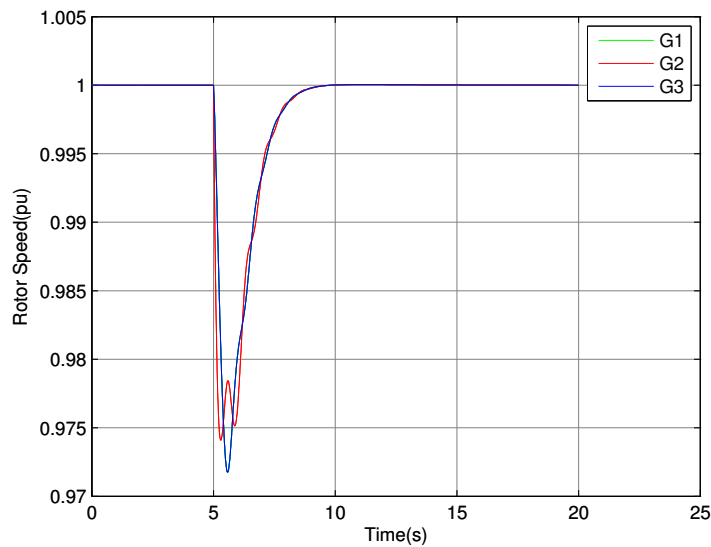


Figure 7.10: Evolution of the Rotor Speed with respect to time

In Figure 7.11, The rotor angles are displayed with respect to a center of inertia reference. One can notice that the rotor angles undergo some oscillations during the first moment of the load sharing and then stabilize to a fixed value which means that the synchronizing torque was enough to keep the DRUPS in synchronism. The rotor angles of DRUPS 1 and 3 are the same during the simulation while the rotor angle is different for DRUPS 2.
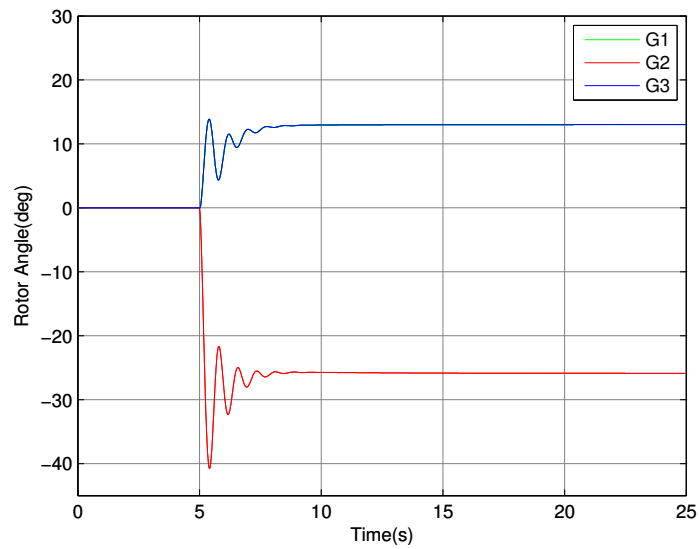
73

Figure 7.11: Evolution of the Rotor Angle of the three DRUPS

For the following test, one will connect a 6 MW load, instead of 5 MW, on the same bus (B21) and this load is almost three times the maximum output power of one DRUPS. As can be seen in Figure 7.12, the DRUPS are losing synchronism few seconds after the disturbance appeared.
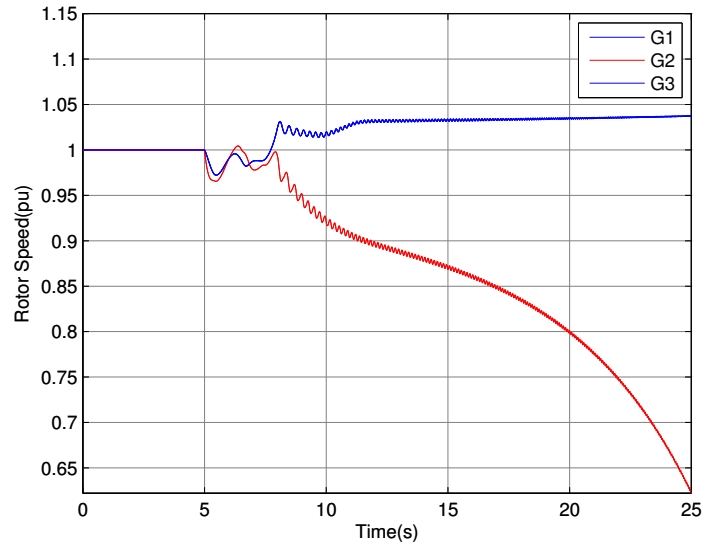


Figure 7.12: Evolution of the Rotor speed of the three DRUPS

This loss of synchronism can be clearly shown in Figure 7.13, the rotor angles can not reach a stabilized value which explained the oscillations of the rotor speeds.
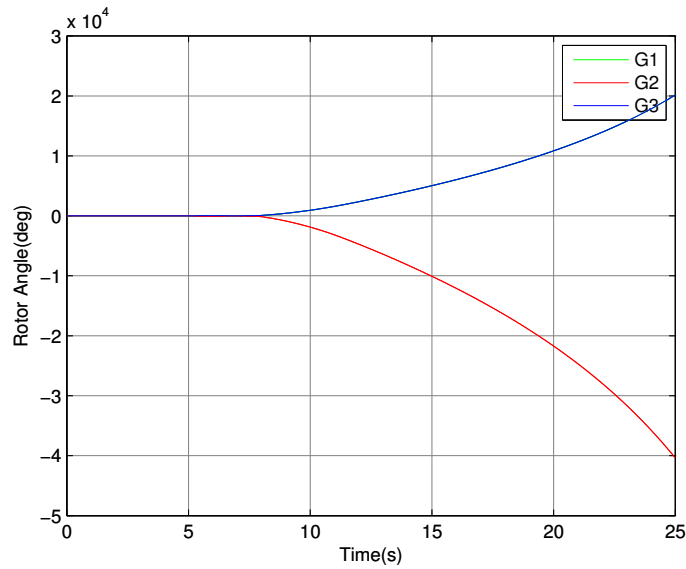
Figure 7.13: Evolution of the Rotor speed of the three DRUPS

One could, intuitively, explain this phenomena by thinking that the synchronizing torque is not enough to maintain synchronism but if one decreases the value of the IP choke, for example at 20 %, the system can find a stable operating point.

In fact, the rotor angle value of the different DRUPS when the system is still stable is a crucial information. Let plot the evolution of the rotor angles of DRUPS 1 (or 3) and DRUPS 2 with respect to different values of load step. As can be seen in Figure 7.14, the green curve is the difference between the blue curve and the red curve. As it can be noticed when the difference is passing 45°, the system becomes unstable, the rotor angles can not stabilize to a fixed value. So, By inspecting the values of the rotor angle, one can determine when the system becomes unstable.
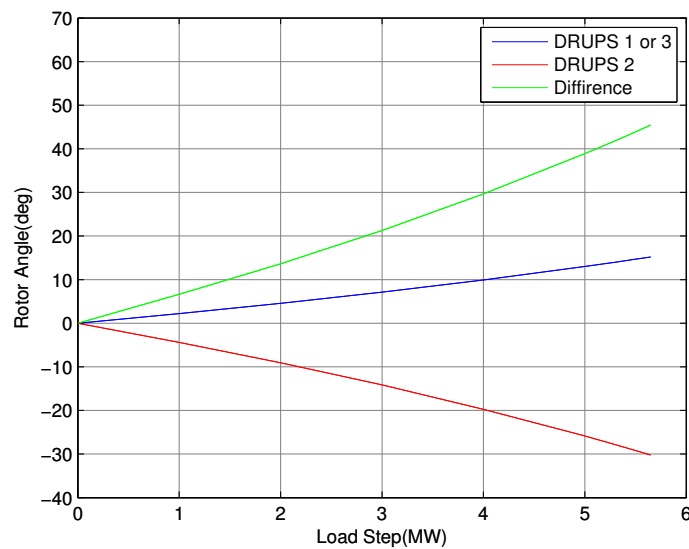


Figure 7.14: Evolution of the Stabilized Rotor Angle with respect to load variation

In conclusion, for those two tests of stability, the value of IP choke chosen has a drastic effect on the step of load that can occur on the load buses. Recall that during the factory test acceptance, it is usual to perform load steps.

**Part IV**

# Euro-Diesel's Strategies

# Marketing Strategy

EURO-DIESEL's product is the NO-BREAK KS® (range power : 100 to 3000 kVA) as discussed in Section 1. The market environment in which EURO-DIESEL is present is called a niche market. So, by being active in such a market, EURO-DISEL aimed at being a big fish in a small pond instead of being a small fish in a big pond. Two main product families have a hand in this niche market : The static UPS and the dynamic UPS. The static UPS are mainly batteries and have a large part of the market, the principal actors and, thus, competitors for EURO-DIESEL are : Schneider Electric, Eaton and Emerson. Concerning the dynamic UPS family where EURO-DIESEL is present, their principal competitors are : Piller, Hitec and Hitzinger.

As discussed, EURO-DIESEL targets a particular market and in Europe, the demand is limited. Therefore, the need to grow worldwide was important for the company. As can be seen in Figure 7.15 [13], EURO-DIESEL is present internationally, the blue dots represent the distributors and the yellow dots represent the subsidiaries.
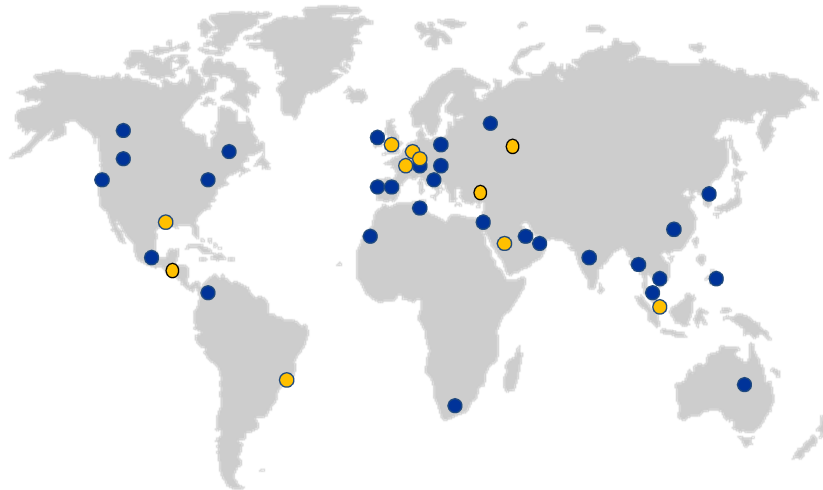


Figure 7.15: The Worldwide Presence of Euro-Diesel

The early strategy of EURO-DIESEL was only to work with distributors but the drawback of this strategy is that the NO-BREAK KS® was a product among others within the distributors. So, they chose, in addition to the distributors, to create subsidiaries across the world in order to thrive. In fact, some problems came with their expansion such that technical constraints, indeed, for some parts of the world, the UPS must resist high temperature and for other parts, the UPS must resist low temperature. EURO-DIESEL also faced other problems such that the adaptation to the culture of different countries and the legislative aspects (import duty...).

To be successful, EURO-DIESEL has been able to adapt their philosophy depending on the country they were settled. The reliability, longevity and efficiency of the product are the strength of EURO-DIESEL.

The commerce in which EURO-DIESEL is involved is a business-to-business commerce. In fact, there are three principal ways to get clients. For the first way, the clients can directly contact EURO-DIESEL by searching them on the web, if one type "Dynamic UPS" on Google, the first link is the EURO-DIESEL's website. For the second way, EURO-DIESEL's salesmen contact potential clients. And for the third way, EURO-DIESEL attend events such as the DCD (DataCenter Dynamics) event.

## After Sales Strategy [14]

After sales service contributes to the success and the well-being of EURO-DIESEL. Indeed, this department generates continuous cash-flow and growth along with the installed base in order to generate continuous share-holder value and cover substantial parts of the company-cost, more specifically in bad times. The service allows to achieve customer satisfaction and to enable new business by excellent relations. For this to work, the department manager must monitor and manage employee motivation pro-actively in order to make sure talent stays within the company and our service level remains constantly excellent without exception.

The employees in this department are mainly engineers. In addition to their technical skills, they should at least speak a foreign language to ease the discussion with the different customers. Indeed, each engineer is assigned to a part of the world and have to manage customers in this part. For Belgium and Luxembourg, the Belgian team is the first level and second level support meaning that they take care of the organizing maintenance visits, machine-breakdown and managing the renewal of maintenance contracts. For the subsidaries and distributors (world-wide), the are a back office support or second level support as can be seen in Figure 7.16, they take care of diagnostics, training, spare parts, contracts on service-levels, updating archives and the ten year overhaul.
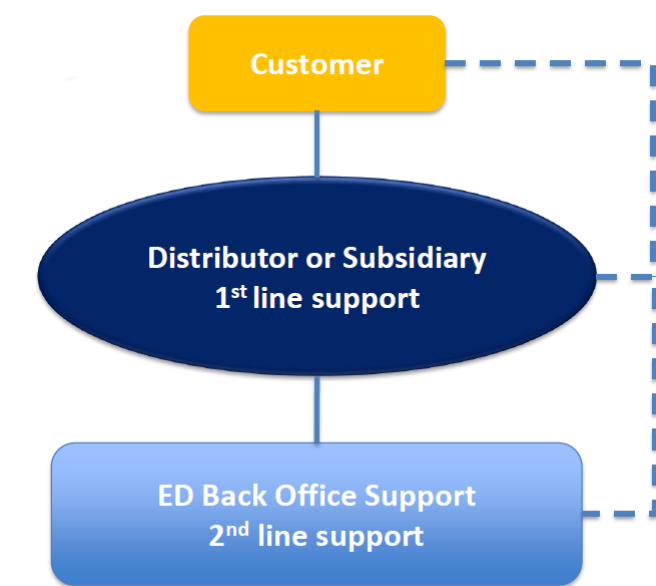


Figure 7.16: Communication with World-Wide Customers

The particularity of this service is that it is a 24 hours on 24 and 7 days on 7 worldwide technical support via phone or via automated alarm transfer. The new technology of the KS-Vision allow to automatically send mails to the back office when a problem arrived to the NO-BREAK KS®. Although, there are seven machine maintenances during a year and every 10 years, an overhaul program is performed, a previously overhauled stato-alternator and the clutch owned by EURO-DIESEL are sent to customers site and are swapped with the original one from the customers site.

## New Strategies

Due to all of these factors discussed previously, EURO-DIESEL is growing every year and thus the human resource employees are looking for qualified people. The parent company of EURO-DIESEL is located in Grâce-Hollogne (Belgium) and employs 125 people (225 across the world). Early 2016, the company was bought out by an investor group called 3I and new strategies are implemented.

The creation of an IT (Information Technology) department was necessary since the communication and the information exchanged between employees are bigger. Before, the information transits were delocalized and time were lost to retrieve certain information. So the IT team want to develop a plan that will make information exchanges optimal and efficient. To gather the information (especially with the subsidiaries), several tools and techniques will be implemented such that the Customer Relationship Management (CRM) or Computerized Maintenance Management System (CMMS). This new strategy will be benefit for the employees working speed.

EURO-DIESEL is setting up a strategy aimed at optimize the workflow (reducing waiting times, reduction of intermediate stock ...) by using a method called the lean manufacturing. In other word, the goal is to reduce the cycle time. The strategy is to make the mechanical workshop the reference model for the other part of the workshop. For that, the supply chain manager will do the mapping process with precise instructions and monitor the mechanical part in the workshop with a tracking sheet.

After more than 80 days in the company I come out with a positive experience. Indeed, the team that supervised my work during my internship was always opened to questions and discussions. This experience allowed me to discover the rhythm of life of a company: discussions between colleagues for cases, meetings ... Moreover it also allowed me to meet people from around the world. I think that, overall, EURO-DIESEL is well-balanced company which is constantly evolving.

# Chapter 8

# Conclusion

Reached the end of this work, we will outline the path that has allowed us to develop a static and dynamic modeling of the NO-BREAK KS® in an IP topology.

The first stage was devoted to describing the operation of the NO-BREAK KS® as well as the description of the different topologies with which we worked.

The second stage, for its part, was dedicated to the static modeling of NO-BREAK KS® in the IP topology. Indeed, a program was developed for the EURO-DIESEL electrical engineering department which solves the power flow equations using the Newton-Raphson procedure. This program would also allow the user to work with a simple input interface and the program is able to automatically perform various scenarios using SCILAB software. This helps to quickly and efficiently obtain essential electrical results to optimize the studied electrical network. Thus, we can easily check if the power of machines is optimal, otherwise, we can readjust the number and power of the DRUPS. In addition, fundamental information about load distribution is given accurately. Simulation of faults has also been implemented which allows the technical department to simulate the effect of a short-circuit on the electrical quantities.

The third stage was to develop the dynamic model of NO-BREAK KS®. To do this, we added to the RAMSES library via CODEGEN utility, the exciter and torque controller models. The response of these models was compared to the response of the real machine during a factory acceptance test to find the PI controller constants. Finally, the models were used to study the stability limits of KS® in the IP topology.

The last stage highlighted the strategies implemented by EURO-DIESEL which allows it to have a good stability on the UPS market especially through the marketing and after sales departments. Emphasize that the implementation of the new IT department will optimize, in the future, the access and transfer of information firstly between the different department and also between subsidiaries distributed throughout the world.

In conclusion, my program allows electrical engineers to EURO-DIESEL to perform faster studies of electrical quantities, pre-fault and post-fault, in the IP topology. Moreover, the developed dynamic models in this master thesis represent rather well the behavior of the engine at the time of occurrence of one or more disturbances and to check whether the electrical system is still stable or not. However, in the future, based on the developments of this thesis, we could consider introducing new features to the current dynamic model.

# Appendix A

# Euro-Diesel's Particular Data

## 1 Negative Reactance Value

In the IP topology, EURO-DIESEL uses a tapped inductor as can be seen in Figure A.1. At both ends, the mains and the load are connected and at the tapped connection the DRUPS is connected.
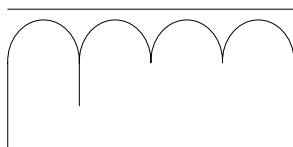


Figure A.1: Tapped Inductor

The tapped inductor can be model as magnetically coupled circuits shown in Figure A.2. The mutual inductance has a negative sign since the current $\bar{I}_2$ leaves the terminal marked by the black dot at the secondary. This negative sign is due to the DRUPS connected at the secondary. Mathematically, we have

$$\begin{bmatrix} \Phi_1 \\ \Phi_2 \end{bmatrix} = \begin{bmatrix} L_{11} & -L_{12} \\ -L_{12} & L_{22} \end{bmatrix} \begin{bmatrix} i_1 \\ i_2 \end{bmatrix}$$

And using the phasor notation of the voltage and the current, we have

$$\begin{bmatrix} \bar{V}_1 \\ \bar{V}_2 \end{bmatrix} = \begin{bmatrix} X_{11} & -X_{12} \\ -X_{12} & X_{22} \end{bmatrix} \begin{bmatrix} \bar{I}_1 \\ \bar{I}_2 \end{bmatrix}$$
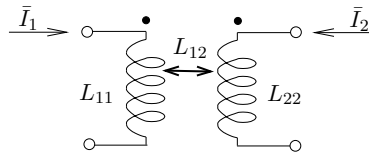
Figure A.2: Magnetically Coupled Circuits

To facilitate numerical simulations, we can use the equivalent circuit shown in Figure A.3.
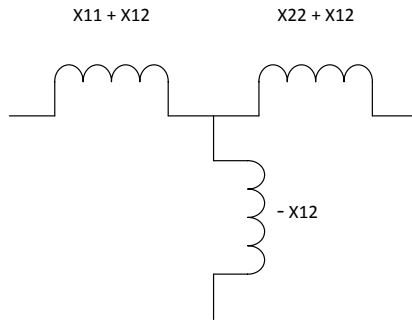


Figure A.3: Equivalent Circuit of the Tapped Inductor

## 2   Dual Cord Load

Some customer's loads can be supplied via two different buses. Half of the power is coming from one bus and the other half is coming from the other bus as shown in Figure A.4.
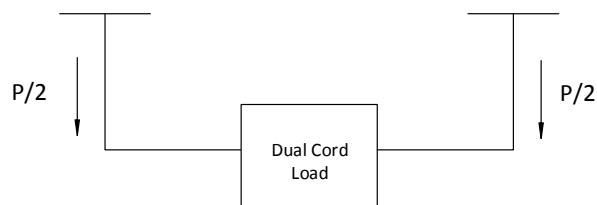


Figure A.4: Supply of the Dual Cord Load

In case of the loss of the left distribution switchboard, the totality of the power consumed by the load must come from the remaining bus as can be seen in Figure A.5.
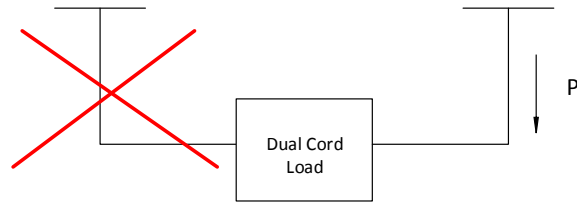
83

Figure A.5: Supply of the Dual Cord Load in Case of the Loss of the Left Distribution Switchboard

For this master thesis, the dual cord power specification is represented by a matrix as follow

Table A.1: Dual Cord Power Specification

|  | Unit 1 | Unit 2 |
|---|---|---|
| Unit 1 | 0 | P/2 |
| Unit 2 | P/2 | 0 |

# References

[1] Euro-Diesel Website. Available on-line : http://www.euro-diesel.com/english/about-us/3/2

[2] Wikipedia Website. Available on-line : https://en.wikipedia.org/wiki/Scilab

[3] Euro-Diesel, "The Leading-EDGE Diesel Rotary Uninterruptible Power Supply System", 2015.

[4] Euro-Diesel, "ISOLATED PARALLEL STAR BUS PRINCIPLE OF OPERATION - TI0020", rev 04.

[5] Euro-Diesel, "ISOLATED PARALLEL RING BUS PRINCIPLE OF OPERATION - TI0021", rev 01.

[6] James D. McCalley, "The Power Flow Problem", Iowa State University. Available on-line : home.eng.iastate.edu/ jdm/ee553/PowerFlow.doc

[7] Yang Liu-Lin, Hang Nai-Shan, Liu Bai-Jiang, "A Modular Approach to Power Flow Regulation Solution", The Open Electrical & Electronic Engineering Journal , 2015, 9:91-98. Available on-line : http://benthamopen.com/ABSTRACT/TOEEJ-9-91

[8] T. Van Cutsem, Electric Power System Analysis, Univ. of Liège, Lecture notes of course ELEC0029, 2016. Available on-line : http://montefiore.ulg.ac.be/ vct/courses.html

[9] Thierry Van Cutsem, Implementing models in RAMSES with the CODEGEN utility, Version 3, May 2016.

[10] Thierry Van Cutsem, Petros Aristidou, "An overview of RAMSES (RApid Multiprocessor Simulation of Electric power Systems)", Univ. of Liège, September 2014. Available on-line : http://www.montefiore.ulg.ac.be/ vct/software.html

[11] IEEE Std 421. 5-2005, "IEEE recommended practice for excitation system models for power system stability studies", IEEE Power Eng. Soc., pp. 14, 2006.

[12] T. Van Cutsem, Power systems dynamics, control and stability, Univ. of Liège, Lecture notes of course ELEC0047, 2016. Available on-line : http://montefiore.ulg.ac.be/ vct/courses.html

[13] Prabha Kundur, "Power System Stability and Control", McGraw-Hill, 1994.

[14] Euro-Diesel, "CERVIN DE CRISTAL 2014 DOSSIER DE PARTICIPATION", 2014.

[15] Strijn Briers, "After Sales Department", Euro-Diesel, 06-01-2016.